SUDAN UNIVERSITY OF SCIENCE AND TECHNOLOGY
COLLEGE OF GRADUATE STUDIES

THEORETICAL STUDY OF ELECTRONIC AND OPTICAL PROPERTIES OF SOME MOLECULES AS POTENTIAL ORGANIC SEMI-CONDUCTORS FOR SOLAR CELL APPLICATIONS

دراسة نظرية للخصائص الإلكترونية والبصرية لبعض المركبات كأشباه موصلات عضوية للتطبيقات فى الخلايا الشمسية

A Thesis Submitted in Fulfillment of the Requirements for the Award of the Degree of Doctor of Philosophy (Chemistry)

by

Zemzem Ali Abdelhasib Ali
B.Sc., MSc.

Supervisor: Dr. Elfatih Ahmed Hassan,
Sudan University of Science and Technology.
Co-Supervisor :Dr. Sahar Shamseldden Abdalla,
University of Khartoum.

September 2022

Dedication

I would like to dedicate my dissertation to my parents.

Acknowledgment

Praise is to Allah, the almighty, who graciously favored me to get over this work and enable me to accomplish this achievement.

I would like to thank and acknowledge my supervisor,

Dr. Elfatih A. Hassan, and co-supervisor, Dr. Sahar S. Abdalla for their vital encouragement and support.

I would like to convey my sincere thanks and appreciation to my colleagues and friends for sharing knowledge and experiences.

Declaration of the Status of Dissertation by Student

*I hereby declare that this dissertation "***THEORETICAL STUDY OF ELECTRONIC AND OPTICAL PROPERTIES OF SOME MOLECULES AS POTENTIAL ORGANIC SEMI-CINDUCTORS FOR SOLAR CELL APPLICATIONS** *" is the result of my own research except the citations in the references. The dissertation has not been accepted for any degree nor concurrently submitted in candidature for any other degree.*

Signature:

Name of the Student:

Date:

Publications from this thesis:

Zamzem **Ali**, Sahar **Abdalla**, Elfatih A. **Hassan**, Yunusa **Umar**, Muneerah Mogren **Al-Mogren**, (2022), Theoretical Study of Electronic and Optical Properties of Functionalized Indigo and Alizarin as Potential Organic Semi-conductors for Solar Cells Applications, *Materials Today Communications*, **32**, p.104048.

Zamzem **Ali**, Sahar **Abdalla**, Elfatih A. **Hassan**, Yunusa **Uma**r, Muneerah Mogren **Al-Mogren**, (2022), A DFT and TD-DFT study on emodin and purpurin and their functionalized molecules to produce promising organic semiconductor materials. *Journal of King Saud University-Science,* **34,** p.102117.

Abstract

The optical and electronic properties of four conjugated organic molecules, Indigo, Alizarin, Emodin and Purpurin, as potential organic solar cells were studied theoretically. The electronic properties, reorganization energy (λh and λe), adiabatic ionization potential (IP), adiabatic electron affinity (EA), chemical hardness (n), highest Occupied Molecular Orbital(HOMO) and Lowest Unoccupied Molecular Orbital(LUMO) energies and HOMO-LUMO energy gap (Eg) were calculated using density functional theory (DFT). The optical properties as the maximum absorption (λmax) along with oscillator strengths (f) at the excited states in vacuum and ethanol as a solvent were also calculated using time-dependent density functional theory (TD-DFT). The impact of functionalization, of these molecules with electronegative functional groups, on their optical and electronic properties was explored. The results show that the values of λh and λe for Indigo were 0.195 eV and 0.175 eV and for Alizarin 0.366 eV and 0.482 eV, respectively.

The functionalization of Indigo and Alizarin has resulted in overall conversion of the materials to better n-type molecules.

The introduction of functional groups to Emodin converted the molecule from p-type into n-type material. while functionalization of Purpurin, which is considered as an n-type material, with NO2 and F- resulted in a slight increase of λe with values of 0.42 eV for each. This is considered as detrimental for the charge-transport process.

The functionalized molecules have shown an increase of EA and decrease in LUMO energy level, indicating their potential use as n-type materials. Overall, the (Eg) for studied molecules has been generally reduced upon introduction of electronegative functional groups. This indicates the possibility of tuning the optical and electronic properties of these organic molecules by introducing suitably selected functional groups. Also, the studied molecules along with their functionalized molecules show properties that fall among organic semi-conductors and thereby, can potentially be used in solar cells.

The intermolecular interaction studies on Emodin and Purpurin, using Hirschfeld surface analysis and energy framework, showed that the major intermolecular interaction occurs at the O– H/H–O with 31.8% for Emodin and 41% for Purpurin.

مستخلص

تم إجراء دراسة نظرية لأربع مركبات عضوية من المحتمل إستخدامها في الخلايا الشمسية وهي: إمودين و إنديغو و بوربيورين و ألايزارين. وباستخدام نظرية الدالة الوظيفية للكثافة (DFT) و تم حساب الخواص الالكترونية التالية: طاقة إعادة التنظيم (λe and λh) ، طاقة التأين الأديباتي , (IP) طاقة الإلفة الألكترونية الاديباتيه (EA) ، الصلابة الكيميائية (n) ، طاقة أعلي مدار جزيئي مشغول (HOMO) ، وطاقة أدني مدار جزيئي غير مشغول (LUMO) ، و الفرق الطاقي بينهما (Eg) . وباستخدام نظرية الدالة الوظيفية للكثافة المعتمدة علي الزمن-DT) (DFTتم دراسة الخواص البصرية وهي أقصي الامتصاص (λ max) مع قوة التذبذب(f) في الحالات المثارة في الفراغ و مذيب الايثانول. كما تمت اضافة مجموعات وظيفية كهروسلبية للجزيئات المستهدفة بالدراسة بغرض تتبع تأثيرهذه المجموعات الوظيفية علي الخواص الالكترونية و البصرية. وقد وجد أن اضافة المجموعات الوظيقية لكل من أنديغو و ألايزارين أدى الى تحويلهما الى أشباة موصلات من النوع (n-type) n ، ولكن الاضافة الى إمودين أدت الي تحويلة الي مركب من النوع (p-type) p ، أما المركب بوربورين، و الذى يصنف بأنه من النوع n فإن إضافة المجموعات NO_2 , F^- أدى الى إرتفاع طفيف فى قيم طاقة إعادة التنظيم (λe)و الذى له تأثير سلبى على عملية نقل الشحن. أوضحت الدراسة بأن هنلك زيادة فى طاقة الالفة الالكترونية الاديباتية (EA) ونقصان فى قيم LUMO فى المركبات التى تم إضافة المجموعات الوطيفية المختلفة لها ، مما يدل على إمكانية إستخدامها كأشباه موصلات من النوع n (n-type).

بشكل عام حدث إنخفاض فى قيم الفرق الطاقى للمركبات التى تم دراستها عند إضافة المجموعات الوظيفية الكهروسلبية ، مما يدل على إمكانية إعادة ضبط الخواص البصرية و الالكترونية باضافة مجموعات وظيفية منتقاه.

وقد أظهرت المركبات الاربعة التى تمت دراستها و مشتقاتها ، الناتجة عن إضافة المجموعات الوظيفية إليها، خواص أشباه الموصلات العضوية مما يعزز إمكانية إستخدامها فى تطبيقات الخلايا الشمسية

وأظهرت دراسة التفاعلات بين-الجزيئية باستخدام تحليل هيرشفيلد السطحى وتحليل الاطار الطاقى ، بأن التداخلات بين-الجزيئية تمت عند O-H/H-O بقدار 31.8% فى إمودين و 41% فى بوربورين.

Table of Content

List of Tables

Page

List of Figures

Abbreviations

OPV	Organic Photovoltaic
HOMO	Highest Occupied Molecular Orbital
LUMO	Lowest Unoccupied Molecular Orbital
FMO	Frontier molecular orbitals
IP	Ionization Potential
EA	Electron Affinity
BHJ	Bulk heterojunction
PCE	Power conversion efficiency
FF	Fill Factor
V_{oc}	Open circuit voltage
J_{SC}	Short circuit current density
P_{inc}	Incident input power
J_{max}	Maximum point current density
V_{max}	Maximum voltage
EQE	External Quantum Efficiency
D–A	Donor - Acceptor
IPCE	Incident Photon to Converted Electron Efficiency
Rs	Series Resistance
Rsh	Shunt Resistance ID Diode
DFT	Density functional theory
TD-DFT	Time-dependent density functional theory
HF	Hartree-Fock
LDA	The Local Density Approximation
SCF	Self-consistent Field
STO	Slater-type Orbital
GTO	Gaussian-type Orbital

GGA Gradient-Corrected Functional

MGGA Meta-gradient corrected.

CHAPTER 1

Introduction

1.1 Introduction

Renewable energy is energy that has been derived from earth's natural resources and acts as alternative for traditional energy sources such as fossil fuels. The production of power from renewable energy sources have increased by 280% since 2006 (Simon 2015), sources of renewable energy includes, hydroelectric power, wind energy, biomass, tidal energy, wave energy and solar energy (Sukhatme & Nayak 2017).

One of the most promising abundant sources of renewable energy is solar energy, the earth receives a total quantity of radiant energy from the sun of 1370 W/m^2/s, with 343 W/m^2/s received per unit area of the Earth's surface (Zaidi 2018). The abundance and non-polluting characteristics of solar energy have made it a widely recognized renewable source of energy. The photovoltaic effect of solar cells can convert this solar energy into electrical energy (S.Ashok n.d.) and it is considered to be one of the most important sources of renewable energy as the world demand of energy increases every year (Bernede 2008, Gupta 2015).

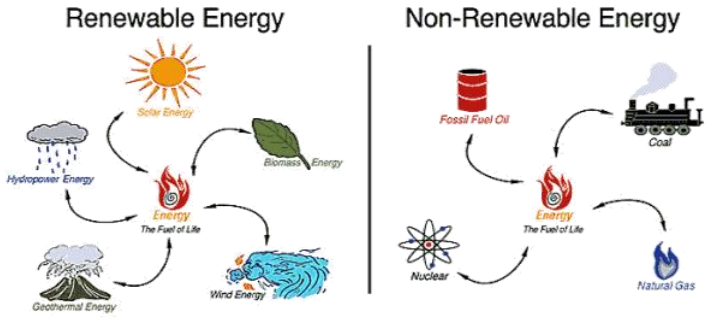

Fig. 1.1. Sources of renewable and non-renewable energy

The photovoltaic effect was discovered by Becquerel in 1839, when he observed a photocurrent when platinum electrodes covered with silver halogen were illuminated in aqueous solution; photoelectrochemical effect (Becquerel 1839). It was in the 1873 and 1876, that the first reports on selenium photoconductivity were made by Smith and Adams (Smith 1873). Further progress was made by reporting the first observation of photoconductvity in organic compound (anthracene) by Pochettino (1906) (Pochettino & Sella 1906) and Volmer (1913) (Volmer 1913). In the late 1950s and 1960s, the potential use of organic solar materials as photoreceptors in imaging system was recognized

(Borsenberger & Weiss 1993). In 1954, the first inorganic solar cell was developed at Bell Laboratories which was based on Si and had an efficiency of 6% (Chapin et al. 1954). Thereafter, tremendous amount of work has been performed to improve the efficiency and reduce the cost of Si solar cell. Although, there have been improvements in the efficiency of the Si solar cell, the cost of production still remains high (Spanggaard & Krebs 2004) unlike the low cost of production of organic solar cells (Bagher et al. 2015, Chen & Chao 2006, Ourahmoun & Belkaïd 2010, Ray et al. 2010).

An organic photovoltaic (OPV) is a type of solar cell that is based on organic semiconductors that includes small organic molecules or oligomers and polymers. It can be classified into p-type and n-type material, the p-type is a material that contains holes as major carrier (hole transporting) and can be prepared from donating π-systems, whereas the n-type contains electrons as the major carrier (electron transporting) and can be prepared from electron-accepting materials (Bao et al. 1998, Chesterfield et al. 2003, Filo & Putala 2010). Some of the most commonly used organic molecules in solar cells include copper phthalocyanine (CuPc), C60 (fullerene), α,α-bis(2,2dicyanovinyl)-quinquethiophene (DCV5T). The CuPc has been used as the electron donor due to it's high stability, high mobility, and abundance. A bulk-heterojunction structure with combination of CuPc:C60 separated by a layer of silver nanoclustors showed high efficiency. Moreover, DCV5T:C60 combination has reached IPCE of 52% leading to overall efficiency of 3.4% (Cravino et al. 2006, Peumans et al. 2003, Uchida et al. 2004). The most important factors to be considered for an effective OPV includes strong light absorption, thermal and photo stability, energy gap between the highest occupied molecular orbital (HOMO) and the lowest occupied molecular orbital (LUMO), abundance and low cost energy(Aubouy et al. 2007, Colley 2016, Scharber & Sariciftci 2013). However, there remains the challenge of enhancing the proficiency of organic solar cells in comparison to inorganic solar cells. Several research efforts are being carried out on organic solar cells systems to improve their efficacy, processing and stability (Arbouch et al. 2014, Jørgensen et al. 2008, Sahdane et al. 2017). These improvements require enhancement of three parameters which are: internal short circuit current (I_{SC}), open circuit voltage (V_{OC}) and fill factor (FF). The I_{SC} is the solar cell maximum current when the voltage is zero, the V_{OC} is the maximum voltage in the solar cell when the current is zero and the FF is the ratio of the maximum power that can be obtained by solar cell to the product of V_{OC} and I_{SC}.

The I_{SC} can be improved by lowering HOMO-LUMO energy gaps of the donor material while the V_{OC} is enhanced by tuning of the energy gap between the HOMO of the donor

material and LUMO of the acceptor material and it is also influenced by the reorganization energy (Cnops 2015).

The reorganization energy (λ) is a reflection of the structural changes that take place when the molecule transfers from neutral to charged (Oshi et al. 2017). There are two types of reorganization energies, the internal reorganization energy (λ_{int}) and external reorganization energy (λ_{ext}). The structural change between ionic and neutral state of the molecule is expressed as λ_{int} and the effect of the external polarized medium is expressed as λ_{ext}. However, the effect of λ_{ext} is considered to be very small that it can be neglected (Sun & Jin 2017, **?**). The reorganization energy is important for the efficient charge generation and transportation, the smaller it's value the greater the charge transport, V_{OC} and FF (Jin & Wang 2015, Ward et al. 2015). Overall, the optical and electronic properties of the organic material play a major role in determining OPV efficiency (Oshi et al. 2017). One of the approaches used is to enhance the optical and electronic properties of organic semiconductor molecules by using functional groups to tune their properties (Oshi et al. 2017). For instances, it was stated that the introduction of electron-deficient atoms or groups increases the molecule electron affinity by reducing the molecular LUMO and thus resulting in better n-type organic semi-conductors. These functional groups include imides, amides, carbonyls, quinone and halogen atoms (Arbouch et al. 2014). To increase the environmental stability and electron affinity of conjugated systems, imides and amides are introduced into the backbone of the molecules as strong electron-withdrawing groups (Meng & Hu 2012). In a study conducted by Zhenan *et al.*, a p-type material, metallopthalocyanine, was converted into n-type air-stable material by functionalization by fluorine (Bao et al. 1998). Other research showed the perfluorination of pentacene converted it into n-type material (Sakamoto et al. 2004) while the chloro (Cl) and nitro (N) functionalization of pentacene and naphthalene provided a better material than perfluoro-pentacene and octafluoro-naphthalene (Chen & Chao 2006, Oshi et al. 2017). The addition of F and CN group to 1,3,5-tripyrrolebenzene (TPB) have stabilized frontier molecular orbital and improved air stability (Hu et al. 2016). In addition, the influence of functionalization on absorption was reported by R. Cardia *et al.*(Cardia et al. 2014) in functionalized triisopropylsilylethynyl (TIPS), resulting in redshifting of the absorption spectrum and improved visible region absorption. The improvement of absorption in the visible region was also shown in different sensitizers functionalized by OH, NH_2, OCH_3, CF_3, F, and CN (Wang et al. 2020).

The effect of functionalization on the reorganization energy has been reported by many studies. For example, Hutchison *et al.*(Hutchison et al. 2005) investigated the

functionalization impact of oligomers of thiophene and furan in terms of reorganization energy. Others have revealed that the cyanation of pentacene gives smaller values of hole (75 meV) and electron reorganization energy (87 meV) than pentacene (94 and 133 meV, respectively) (Kuo et al. 2007). Oshi and co-workers discussed the increase of hole and electron reorganization energy in 7,7,8,8-Tetracyanoquinodimethane by electron donating groups CH_3, OCH_3, and OH (Oshi et al. 2019). Thus, it is valuable to recognize the effect of functionalization on molecule's reorganization energy as it provides perception into charge transfer rate in organic semiconductor materials.

The charge transport (at low temperatures) in organic semiconductors is described as band-like motion in which the charge is delocalized across the system. The charge transport technique at high temperatures is represented by a hopping mechanism where the charge transporters are localized to a single molecules, and jump from a molecule to a nearby molecule as described by the Marcus equation, which is given as follows (Marcus 1993, Ottonelli et al. 2012).

$$K = (4\pi^2/h)t^2(4\pi\lambda K_B T)^{-0.5} exp[-\lambda/4K_B T]$$

where h is the Planck constant (6.626 × 10−34J.s), t is the charge transfer matrix element, λ is the charge reorganization energy, KB is Boltzmann constant and T is the absolute temperature. The charge transport rate from the equation is mostly affected by the reorganization energy and electronic coupling (transfer integral). The charge transport rate is determined by the transfer integral, which in influenced by the orientation and distance of the molecules. A lower reorganization energy land larger transfer integral that lead to a faster charge transport rate (Brédas et al. 2002, Chen et al.2017, Gruhn et al. 2002).

Due to the development need of OPV, there has been a continuous design and testing of different organic semi-conductor materials and to date several materials have been investigated (Arbouch et al. 2014, Jin & Wang 2015, Oshi et al. 2018, 2019, Ottonelli et al. 2012, Ourahmoun & Belkaïd 2010, Sun et al. 2016, Sun & Jin 2017). The theoretical study of these molecules aids in the rational designs of efficient OPV and screens potential organic semiconductors for solar cells (May 2012). In this research, the influence of functionalization on electronic and optical properties of four conjugated molecules Indigo (2,2'-Bis(2,3-dihydro-3-oxoindolyliden)),Alizarin *(1,2Dihydroxyanthracene-9,10-dione)*, Emodin *(6-methyl-1,3,8-trihydroxyanthraquinone)* and Purpurin

(1,2,4-Trihydroxyanthraquinone) are studied to understand their possible use in organic solar cells, Fig 1.8, Fig 1.9, Fig 1.10 and Fig 1.11, respectively. The molecules are investigated as potential organic semi-conductors due to their abundance as they are used as colorants and their intense colors indicate a high degree of light absorption and an extensive electron resonance and delocalization in molecular orbitals (Prabha et al. 2017).

1.2 OPV Operating Principle

An OPV is based on organic semiconductors that includes small molecules or oligomers and polymers. The conjugated system of the molecules is formed by the covalent bonding with alternating sequence of carbon atoms with single-double and/or single-triple bonds. The overlapping between two parallel p orbitals forms a bonding π orbital with a π_* anti-bonding orbital. The delocalization character of π and π_* orbitals in conjugated systems give rise to delocalized frontier molecular orbitals called the highest occupied molecular orbital (HOMO) and the lowest unoccupied molecular orbital (LUMO) (Arbouch et al. 2014).

The basic operating principle of organic cells is the initial absorption of photons with sufficient energy that leads to the promotion of an electron to the LUMO level and leaves a hole on the HOMO, forming electron-hole pair known as exciton. Excitons are formed because of the low dielectric constant of organic semiconductors which results into high coulombic force and attraction between the photo-generated electrons and holes (Garcia-Belmonte et al. 2008). The formed excitons must be dissociated in order to produce and transport free charge carriers throughout the organic device. This is accomplished by creating a heterojunction between two dissimilar organic semiconductor materials; donor (n-type) and acceptor (p-type). A donor is defined as a material that has a high ionization energy (IP) and an acceptor is a material that has a high electron affinity (EA). After excitation of the electron from the HOMO to the LUMO, the electron can jump from the LUMO of the donor (material with higher LUMO) to the LUMO of the acceptor (material with lower LUMO) if the potential difference between the ionization potential (IP) of the donor and the electron affinity (EA) of the acceptor is larger than the exciton binding energy (Arbouch et al. 2014). The excitons formed on the donor material can be dissociated at the donor-acceptor interface, the differences in electron affinities creates a driving force at the interface between the donor and acceptor that is strong enough to separate the charges. However, the produced exciton must reach the interface before the excitation energy of the exciton is lost via intrinsic radiative and non-radiative decay process to the ground state. To facilitate the dissociation, the donor and acceptor should

be in a close proximity with optimum length scale that is in the range of the exciton diffusion length and the thickness of the active layer should be comparable to the penetration length of the incident light which is typically 80 - 200 nm. The hole should also remain on the donor due to its higher HOMO level as the exciton may transfer itself completely to the material of lower-band gap accompanied with energy loss (Kietzke 2007). The energy level offset of the LUMO of the donor material and the acceptor provides the needed energy to break-up the exciton bounding energy. Finally, upon the dissociation of excitons, the electron is transferred to the acceptor material and then to the cathode of charge collection and the hole is transferred to the anode charge collection to initiate current (Arbouch et al. 2014). The presence of excitons in close proximity to an interface increases the chances of separation and transfer to electrodes, the overall process efficiency is describes by Incident Photon to Converted Electron Efficiency (IPCE). The IPCE is calculated by the number of electrons leaving the device under short circuit condition per time and area divided by the number of photons incident per time and area, it is represented as following:

$$IPCE = \frac{No.ofextractedelectrons}{No.ofincidentphotons}.$$

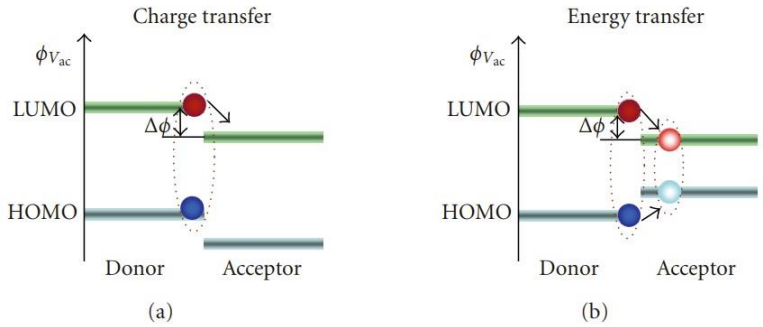

Fig. 1.2. The interface between two different semiconducting polymers (D = donor, A = acceptor) can facilitate either charge transfer by splitting the exciton or energy transfer, where the whole exciton is transferred from the donor to the acceptor(Kietzke 2007)

1.2.1 Manufacturing

One of the important roles in determining OPV efficiency is packaging. The OPV packing commonly takes place as a bi-layer heterojunction of donor-acceptor materials (Nelson 2002, Tang 1986) which can be prepared by subliming or by spin-coating a second layer on the top of the first that lead to a more or less diffused bi-layer structure. This structure

also reduces the chances of charge recombination since the charge carriers travel through pure n-type and p-type layer (Jenekhe & Yi 2000).

Another common way of packaging include a blend of donor and acceptor materials dispersed through the photoactive region, known as bulk heterojunction (BHJ) (Yu et al. 1995). The structure results in a higher interfacial areas and thus improves exciton dissociation efficiency, it can be deposited by co-sublimation of small molecules (Kietzke 2007). In general, the manufacturing procedure for OPV can be classified into two techniques:

- Dry thermal evaporation

- Wet solution processing: spin coating, ink jet, screen print, roll to roll printing and slot-die coating.

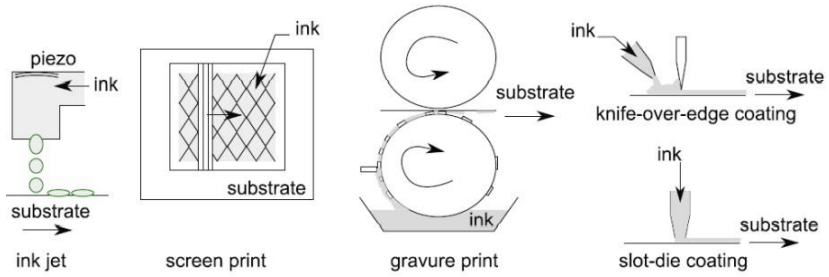

Fig. 1.3. Wet solution processing (Tress 2014)

1.3 Performance Characteristic

The solar cell maybe represented as a simple diode with the following equivalent electric circuit:

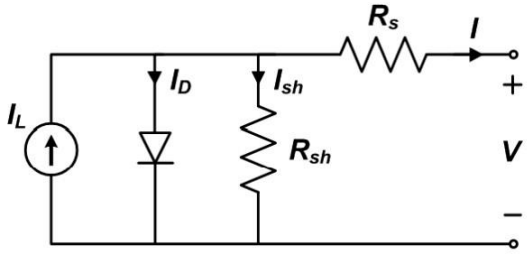

Fig. 1.4. Equivalent circuit for OPV (Jain & Kapoor 2005)

The circuit consists of:

•A diode with I_D current

•A current source that corresponds to photocurrent I_L generated during illumination

•R_s series resistance

•R_{sh} shunt resistance with I_{sh} leakage current through resistance as a result of defects in the films.

For an acceptable performance, a low R_s and a high R_{sh} is required. Upon illumination, the current-voltage (IV) curve becomes a superposition of the dark IV with the light generated current and the curve is shifted down the fourth quadrant, Fig 1.7.

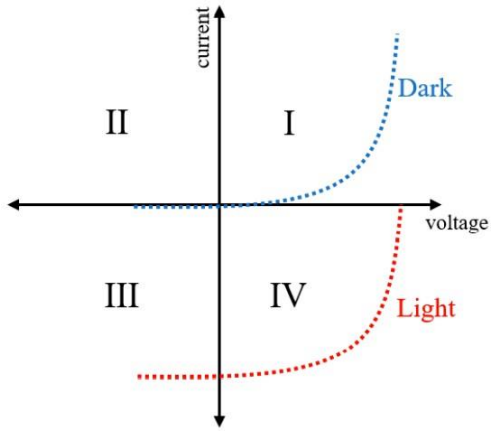

Fig. 1.5. Dark and light IV curves for an OPV (Hamakawa 2003)

One of the most important OPV evaluation metric is Power conversion efficiency (PCE). The PCE is measured in international standard test conditions, under 25 ◦ C and an irradiation of 1000 W/m^2 with an air mass 1.5 spectrum (AM 1.5). The PCE is defined as following:

$$\eta = \frac{P_{max}}{P_{inc}} = \frac{FF \times V_{oc} \times J_{SC}}{P_{inc}}$$

where FF is fill factor, V_{oc} is open circuit voltage, J_{SC} is short circuit current density, P_{inc} is incident input power, J_{max} is the maximum point current density and V_{max} is the maximum voltage (Arbouch et al. 2014). Thereby, the FF, V_{oc} and J_{SC} are the 3 important parameters that determines the PCE of photovoltaic device.

1.3.1 Fill Factor (FF)

The series resistance (R_s), shunt resistance (R_{sh}) and diode (I_D) are the three fundamental elements in the solar cell equivalent circuit that determines the FF. Ideally, the maximum power produced by the cell under illumination is equal to the product of J_{SC} and V_{oc}. However, in practice the diode deviates from the ideal situation and the maximum power becomes the product of the J_{max} and V_{max} (Arbouch et al. 2014). Thus, it is defined as the ratio of the maximum power from the cell over the product of V_{oc} and J_{SC}. Graphically, the FF is represented as the area of the largest rectangle that fit in the IV curve, Fig 1.7.

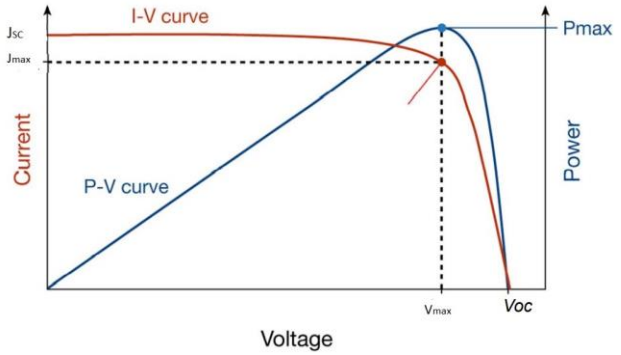

Fig. 1.6. IV curve and maximum power (Selman & Mahmood 2016)

$$FF = \frac{V_{max} \times J_{max}}{V_{oc} \times J_{SC}}$$

Whereas, J_{max} is the maximum point current density and V_{max} is the maximum voltage, V_{oc} is open circuit voltage and J_{SC} is short circuit current density.

1.3.2 Open Circuit Voltage (V_{oc})

The V_{oc} is the difference of the electrical potential between two terminals when a device is disconnected from any circuit (Arbouch et al. 2014). The V_{oc} of solar cell is usually measured under specific condition such as illumination and temperature, it can be increased by increasing ionization potential; the band gap and decreasing the driving force for hole and electron transfer (Markvart et al. 2003).

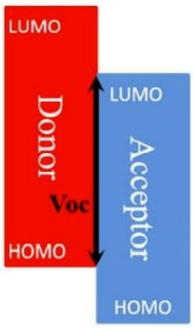

Fig. 1.7. Open circuit voltage VOC for OPV (Markvart et al. 2003)

1.3.3 Short Circuit Current Density (J_{SC})

The J_{SC} is the maximum photocurrent density which can be obtained from the device at short circuit condition. The J_{SC} is the result of generation and collection of light-generated carriers, it is the largest current that can be drawn from the cell and directly proportional to the light intensity. For an ideal solar cell, J_{SC} and the light generated current should be identical. It is related to the external quantum efficiency (EQE) through the following equation (Arbouch et al. 2014) :

$$J_{SC} = \frac{q}{\hbar c} \int_{\lambda_{max}}^{\lambda_{min}} EQE(\lambda) \times P_{inc}(\lambda) \times d\lambda$$

where q is an electron charge, $\hbar$ is the Planck constant, c is the speed of light and λ is the wavelength of the light. The EQE is the ratio of the number of incident photons at a specific wavelength.

Thereby, the EQE depends on five parameters:

- The device efficacy in photon absorption
- The exciton capacity to diffuse to D/A interface
- The efficiency of exciton to dissociate
- The charge carrier transport throughout the device

• The electrodes charge collection efficiency.

1.4 Studied Molecules

1.4.1 Physical and Chemical Properties

1.4.1.1 Indigo

Indigo is 2,2'-Bis(2,3-dihydro-3- oxoindolyliden) a dark-blue powder with coppery luster Fig 1.8. It has a molecular weight of 262.26 g/mol, it is insoluble in water and soluble in aniline, nitrobenzene, choloroform and sulfuric acid with melting point of 734 to 738 ◦F. It is an organic molecule used as a colorant for textiles, apparel, and leather manufacturing. The molecule is produced by condensation of aniline, formaldehyde and hydrocyanic acid to form N-phenylglycinonitrile, followed by alkaline hydrolysis to yield N-phenylglycine which makes indigo in 94 % (n.d.a).

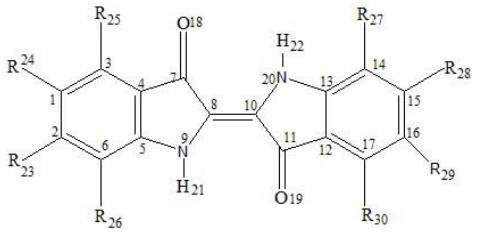

Fig. 1.8. Structure and numbered atoms of Indigo, 2,2'-Bis(2,3-dihydro-3- oxoindolyliden)
Molecule 1: R_{23}= R_{24}= R_{25}= R_{26}= R_{27}= R_{28}= R_{29}= R_{30}=
H Molecule 2: R_{24}= R_{28}= NO_2
Molecule 3: R_{24}= R_{28}= CN
Molecule 4: R_{23}= R_{24}= R_{25}= R_{26}= R_{27}= R_{28}= R_{29}= R_{30} = F
Molecule 5: R_{23}= R_{24}= R_{28}= R_{29}= F
Molecule 6: R_{23}= R_{24}= R_{25}= R_{26}= R_{27}= R_{28}= R_{29}= R_{30} = Cl
Molecule 7: R_{23}= R_{24}= R_{28}= R_{29}= Cl

1.4.1.2 Alizarin

Alizarin is 1, 2 -Dihydroxyanthracene-9, 10-dione, an orange-red crystals or powder, Fig 1.9. It has a molecular weight of 240.21 g/mol, it is sparingly soluble in water and soluble in chloroform and hexane with melting point of 534 to 541 ◦F. It is an organic molecule that has a role as chromophore, a dye and plant metabolite. The molecule is produced by oxidation of anthraquinone-2-sulfonic acid (n.d.b).

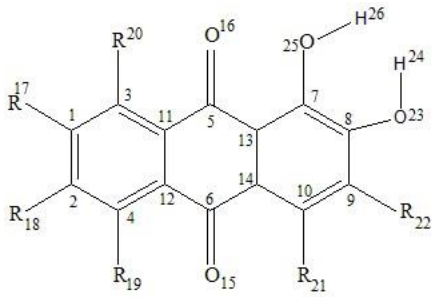

Fig. 1.9. Structure and numbered atoms of Alizarin, 1, 2 -Dihydroxyanthracene-9, 10-dione and it's functionalized molecules.
Molecule 1: R_{17}= R_{18}= R_{19}= R_{20}= R_{21}= R_{22}= H
Molecule 2: R_{17}= R_{18}= R_{19}= R_{20}= Cl
Molecule 3: R_{17}= R_{18}= Cl
Molecule 4: R_{17}= R_{18}= F
Molecule 5: R_{17}= R_{18}= R_{19}= R_{20}= F
Molecule 6: R_{17}= R_{18}= CN
Molecule 7: R_{17}= R_{18}= R_{19}= R_{20}=
CN Molecule 8: R_{17}= NO_2

1.4.1.3 Emodin

Emodin is 6-methyl-1,3,8-trihydroxyanthraquinone, an orange need or powder, Fig 1.10. It has molecular weight of 270.24 g/mol, it is insoluble in water, soluble in ethanol and moderately souble in aqueous alkali solutions with melting point of 493 to 495 ◦F. It is present in the roots and barks of several plants, moulds and lichens and used as cathartic and dye intermediate (n.d.c).

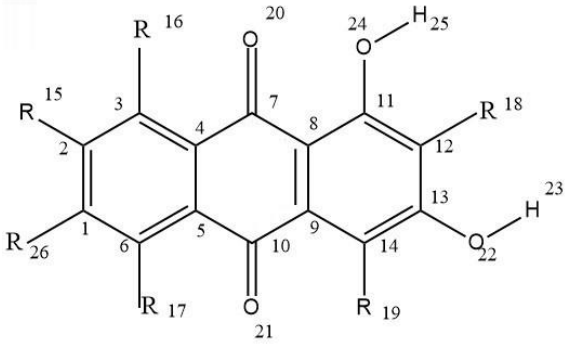

Fig. 1.10. Structure and numbered atoms of Emodin, 6-methyl-1,3,8-trihydroxyanthraquinone
Molecule 1: R15= R16= R17= R18= R19= R26= CH3
Molecule 2: R26= C_2H_5
Molecule 3: R15= CN
Molecule 4: R15= F
Molecule 5: R26= Cl

1.4.1.4 Purpurin

Purpurin is 1,2,4-Trihydroxyanthraquinone,crystalline solid, Fig 1.11. It has molecular weight of 256.21 g/mol, it is insoluble in hexane and soluble in chloroform with melting of 498 ◦F. It is used as a biological pigment, a histological dye and a plant metabolite. It is derived from 9,10-anthraquinone by replacement of three hydrogen atoms by hydroxyl groups (n.d.d).

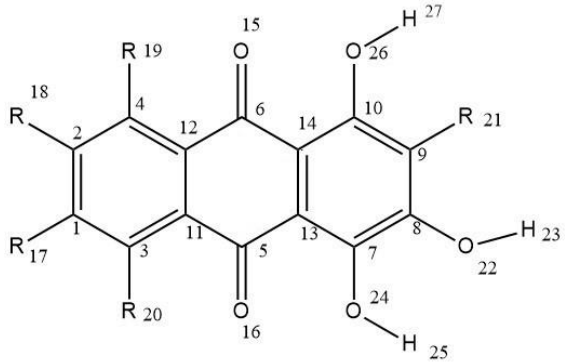

Fig. 1.11. Structure and numbered atoms of Purpurin, 1,2,4-Trihydroxyanthraquinone
Molecule 1: R17= R18= R19= R20= R21= H
Molecule 2: R18= NO_2
Molecule 3: R18= CN
Molecule 4: R18= Cl
Molecule 5: R17= R18= Cl
Molecule 6: R17= R18= F

CHAPTER 2

2 Theoretical Background

2.1 Schrödinger Equation

In the 20th century, physicist discovered that microscopic particles such as electrons and nuclei do not obey the classical mechanics laws. These particles behavior can be described by Quantum Mechanics, the laws of mechanics were discovered by Heisenberg, Born and Jordan in 1925 and Schrödinger in 1926.

Quantum mechanics considers a particle to be distributed through space like a wave, the mathematical expression of the wave is called a wave function, ψ (psi). The Schrödinger equation is used to find the wavefunction of any system. The time-independent Schrödinger equation for a particle of mass m moving in one dimension with energy E is represented by (Atkins & De Paula 2006):

$$-\frac{\hbar^2}{2m}\frac{d^2\psi}{dx^2} + V(x)\psi = E\psi$$

The total energy E is summation of potential and kinetic energy, the first term is related to the kinetic energy where $\hbar$is modification of Planck's constant:

$$\hbar = \frac{h}{2\pi} = 1.05457 \times 10^{-34} Js$$

where the $V(x)$ is the potential energy of the particle at the point x.The potential energy consists of nucleus-electron potential, the electron-electron potential, and the nucleus-nucleus potential.

2.2 Hamiltonian Operator

The Schrödinger equation can also be represented by:

$\hat{H}\psi = E\psi$

where $\hat{H} = -\frac{\hbar^2}{2m}\nabla^2 + V$, and $\nabla^2 = \frac{\partial^2}{\partial x^2} + \frac{\partial^2}{\partial y^2} + \frac{\partial^2}{\partial z^2}$

For the evolution of the system with time, the time-dependent Schrödinger equation is used:

$$\hat{H}\psi = i\hbar\frac{\partial\psi}{\partial t}$$

The $\hat{H}$ is known as Hamiltonian operator, it carries out mathematical operation by taking the second derivative of ψ, then multiplies by $-\frac{\hbar^2}{2m}$ and adds the result to the outcome of multiplying ψ by V. It corresponds to the total energy of the system that includes the kinetic and potential energies.The Hamiltonian for a molecule consisting of n electrons and N nuclei can be represented as(Lewars 2003):

N

$\hat{H} = -\frac{\hbar^2}{2}\sum_{I}$

2.3 Electronic Structure Methods

Quantum mechanics is used to describe the electronic structure of an atom that is essential in understanding the structures and reactions of atoms and molecules. The Schrödinger equation can be solved exactly for a one-electron atom such as Hydrogen but it is extremely complicated for manyelectron atom due to the electron interaction with one another. Thereby, different approaches are used in making approximations (Atkins & De Paula 2006).

2.3.1 Born-Oppenheimer

Born-Oppenheimer is one of the simplest adopted approximations. It suggests that the nuclei, being heavier than the electron, move relatively slowly and may be treated as stationary while electron move in their field. Therefore, the nuclei is considered as fixed at arbitrary locations, and then solve the Schrödinger equation for the wavefunction of electrons only. This approximation allows the separation of the nuclear variable from the electron variables. The Hamiltonian operator obtained after applying the Born-Oppenheimer approximation can be written as sum of the kinetic (T) and potential energies (V) of the nuclei and electrons (Lewars 2003).

$Htot = Tn + Te + Vne + Vee + Vnm$

2.3.2 Hartree-Fock (HF) Theory

Hartree-Fock theory is considered to be one of the simplest kind of ab initio calculations. It is represented by a function called Hartree product which is the product of one-electron wavefunction:

$\psi_0 = \psi_0(1)\psi_0(2)\psi_0(3)....\psi_0(n)$

Where ψ_0 is a function of all the electrons in the atom, $\psi_0(1)$ is a function of the coordinates of electron 1, $\psi_0(2)$ is a function of the coordinates of electron 2...and so on. The initial guess of ψ_0 is based on the zeroth approximation, then we solve for electron 1 a one-electron Schrödinger equation in which electron-electron repulsion comes from electron 1 and an average field of other

electrons, the only moving particle in this equation is electron 1. Then electron 2 is solved for in the same way continuing to electron *n*, the completion of the first cycle of calculation gives (Lewars 2003)

$\psi_1 = \psi_1(1)\psi(2)\psi(3)...\psi_1(n)$

The repetition of the cycle gives,

$\psi_2 = \psi_2(1)\psi_2(2)\psi_2(3)...\psi_2(n)$

The process is repeated for *k* cycles for ψ_k until no change is seen in the ψ values, a procedure known as self-consistent field procedure, SCF. However, the Hartree product address the electron spin in an ad hoc way and the product is symmetric. These disadvantages were corrected by Fock and Slater in 1930, in which the Hartree's iterative, average-field is corrected by electrons spin and antisymmetry leading into Hartree-Fock equation.

2.3.3 Density Functional Theory

The Density functional theory, DFT, is an alternative to wavefunction which is based on electron density function that is known as the electron density or the charge density denoted as ρ. Unlike the wavefunction method that is based on 4*n* variables; three spatial coordinates and one spin coordinate, the electron density is based only on three variable (*x*,*y*,*z*) (Atkins & De Paula 2006, Lewars 2003, Young 2004).

The DFT calculation is based on two theorems set by Hohenberg and Kohn in 1964, the first theorem states that the properties of a molecule in a ground electronic state are calculated by the ground state electron density function $\rho(x,y,z)$.

$\rho_0(x,y,z) \rightarrow E_0$

In which E_0 is a functional of $\rho_0(x,y,z)$, any ground state property of a molecule is a functional of the ground state electron density function, for example, the energy

$E_0 = F[\rho_0] = E[\rho_0]$. The second theorem is based on variation theorem in which the trial electron density will give energy that is higher or equal to the true ground state energy.

$E_v[\rho_t] \geq E_0[\rho_0]$

In which the E_v is the energy of the electrons moving under the potential of the atomic nuclei, ρ is a trial electronic density and $E_0[\rho_0]$ is the true ground state energy corresponding to the true electronic density ρ_0.

In order to determine the electron density the Kohn-Sham approaches DFT by expressing the molecular energy as a sum of terms and use initial guess of the electron density ρ in the KS equation to calculate the initial guess of the KS orbitals and energy levels.

The ground state electronic energy of the real molecule is expressed as the sum of the total electron kinetics energies, the $E_{p;e,N}$ nucleus-electron attraction potential energies and the E_P ;*e*,*e* electronelectron repulsion potential energies and the exchange correlation energy; takes the spin effect into consideration:

$E[\rho] = E_K + E_{p;e,N} + E_P;e,e + E_{XC}[\rho]$

The orbitals that used are used to construct the electron density

$$\rho(r) = \sum_{i=1}^{N} |\psi_i\ (r)|^2$$

are calculated from the Kohn-Sham equations:

$$\Big\{ -\tfrac{\hbar^2}{2m_e}\nabla_1^2 - \sum_{j=1}^{N} \tfrac{Z_j e^2}{4\pi\epsilon_0 r_{j1}} + \int \tfrac{\rho(r_2)e^2}{4\pi\epsilon_0 r_{12}} dr_2 + V_{XC}(r_1) \Big\} \psi_i(r_1) = \epsilon_i \psi_i(r_1)$$

$-\frac{\hbar^2}{2m_e}\nabla_1^2$ = Kinetic energy

$\sum_{j=1}^{N} \frac{Z_j e^2}{4\pi\epsilon_0 r_{j1}}$ = Electron-nucleus attraction

$\int \frac{\rho(r_2)e^2}{4\pi\epsilon_0 r_{12}} dr_2$ = Electron-electron repulsion

$V_{XC}(r_1)$ = Exchange correlation, is the functional derivative of the exchange correlation energy: $V_{XC}[\rho] = \frac{\delta E_{XC}[\rho]}{\delta \rho}$

The equations of Kohn-Sham are solved iteratively and self-consistently in which the electron density is first guessed, superposition of atomic electron densities is commonly used. Secondly, the exchange-correlation potential is calculated by considering approximation of the reliance of the exchange-correlation energy on the electron density and evaluation of the functional derivative of $V_{XC}[\rho] = \frac{\delta E_{XC}[\rho]}{\delta \rho}$. The simplest approximation is the local-density approximation as following:

090 $E_{XC}[\rho] = \int \rho(r)\epsilon_{XC}[\rho(r)]dr$

The ϵ_{XC} is the exchange-correlation energy per electron in a homogeneous gas of constant density. An initial set of orbitals is obtained by solving Kohn-Sham equation, the process of iteration is repeated until the density and the exchange-correlation energy are constant (Atkins & De Paula 2006). The time-dependent density functional theory (TD-DFT) is based on time-dependent Schrödinger equation which can be used in the calculation of UV spectra (Lewars 2003).

2.3.4 The Local Density Approximation (LDA)

The local density approximation, LDA, is the simplest type of exchange correlation energy $E_{XC}[\rho(r)]$ approximation introduced by Kohn and Sham. It assumes that the density can be treated locally as an uniform electron gas; the exchange correlation energy at each point in the system is the same as that of an uniform electron gas of the same density.

The LDA method has been largely replaced by a developed method known as local spin density approximation, LSDA. The LSDA, often known as LSD sets electrons of α and β spin into different Kohn-Sham orbital ψ_α^{KS} and ψ_β^{KS} in which different density functions follows, ρ^α and ρ^β. The functional can handle systems with one or more unpaired electrons such as radicals (Cramer & Bickelhaupt 2003, Lewars 2003).

2.3.5 Gradient-Corrected Functional

In gradient-corrected functional or generalized-gradient approximation, GGA the exchange-correlation energy functional uses the electron density and its gradient; the first derivative of ρ with respect to position, $(\frac{\partial}{\partial x} + \frac{\partial}{\partial y} + \frac{\partial}{\partial z})\rho = \nabla\rho$. Examples of gradient-corrected correlation-energy functionals are the LYP (Lee-Yang-Parr) and the P86 (Perdew 1986) functionals. Functionals that use the second derivative of $\rho(\frac{\partial^2}{\partial x^2} + \frac{\partial^2}{\partial y^2} + \frac{\partial^2}{\partial z^2})\rho = \nabla^2\rho$ are known as meta-gradient corrected, meta-GGA,MGGA.

The MGGA functional depends on the kinetic energy density τ that is obtained by summing the squares of the gradients of the Kohn-Sham MOs (Lewars 2003):

$$\tau(r) = \tfrac{1}{2} \sum_{i=1}^{occupied} |\nabla \psi_i^{KS}(r)|^2$$

Examples of MGGA functionals are τHCTH (Hamprecht, Cohen, Tozer, Handy) and B98 (Becke 1998).

2.3.6 hybrid or Hyper-GGA methods

In hybrid GGA method, the $E_{XC}(\rho)$ is considered as the sum of DFT exchange-correlation energy and HF exchange energy. The percentage of HF exchange energy to use is based on the several hybrid functionals, an example of hybrid-GGA is the B3LYP. In hybrid meta-GGA, the hartree Fock exchange is add on to meta-GGA, the first and second derivative of ρ and Hartree-Fock exchange (Lewars 2003).

2.4 Basis Sets Approximation

A basis set is a set of mathematical functions (basis functions) that describes system orbital used in approximating theoretical calculations or modeling. The most commonly used functions are Slatertype orbital (STOs) and Gaussian-type orbital (GTOs), the STOs functions are used in semiempirical methods and the gaussian functions are used in ab initio methods.

The general expression of STOs is given as following (Lewars 2003):

$STOs = N \times e^{-\alpha r}$

where N is the normalization constant, α is the orbital exponent and r is the radius in angstroms.

STOs are described by function depending on spherical coordinates:

$\phi_1(\alpha,n,l,m;r,\theta,\phi) = Nr^{(n-1)}e^{-\alpha r}Y_{l,m}(\theta,\phi)$

The r,θ and ϕ are spherical coordinates, and $Y_{l,m}$ is the angular momentum. The n,l and m are quantum numbers, principal, angular momentum and magnetic, respectively.

The STOs implementation on two-electron integrals requires excessive computer time and becomes extremely difficult to calculate, however, they can be evaluated by Gaussian basis functions. The GTOs uses easier evaluated functions in which the exponential $e^{-\beta r2}$ rather than the STOs $e^{-\alpha r}$. It is represented as following:

$$G_{i,j,k} = N x_a^i y_a^j z_a^k e^{-\alpha r_a^2}$$

where i,j and k are non-negative integers, α is a positive orbital exponent, x_a,y_a, and z_a are Cartesian coordinates with the origin at a, and N is the Cartesian Gaussian normalization constant.

Basis set can be classified into the following (Lewars 2003, Ramachandran et al. 2008):

- Minimal basis sets: One basis function for every atomic orbital that is required to describe the free atom is selected. This includes STO-3G, STO-4G,STO-6G,STO-3G* (polarized)
- Pople basis sets: Each basis function is represented as a sum of gaussian primitives, 3-21g, 3-21g* (polarized), 3-21+g (Diffuse), 3-21+g* (polarized and diffused), 6-31g,6-31g*,6-31+g*, 6-31g(3df, 3pd), 6-311g, 6-311g*, 6-311+g*
- Correlation consistent basis sets: These are basis sets that includes shells of polarization (correlating) functions that can converge the electronic energy to the complete basis set limit such as cc-pVDZ, cc-pVTZ, cc-pVQZ, cc-pV5Z, aug-cc-pVDZ
- Double, triple and quadruple zeta basis sets: These are basis sets that have several basis functions for each atomic orbital that includes both inner and valence orbitals, known as zeta basis sets. Example is D95 basis set of Dunning.
- Plane wave basis sets.

2.5 Hirschfeld Surface Analysis

Molecules within a crystal structure may utilize Hirschfeld surface analysis to determine the intermolecular interactions between particular molecules or for the crystal structure. The space in the crystal is partitioned into regions where the electron distribution of a sum of spherical atoms for the molecule (the promolecule) dominates the corresponding sum over the crystal (the procrystal) to construct the Hirschfeld surface of a molecule. The molecular weight function $w(r)$ is defined as (Spackman et al. 2021b):

$$w(r) = \frac{\rho_{promolecule}}{\rho_{procrystal}}$$

$$w(r) = \frac{a_\epsilon \sum\limits_{molecule} \rho_a(r)}{b_\epsilon \sum\limits_{crystal} \rho_b(r)}$$

$\rho_a(r)$ is a spherically-averaged atomic electron density centred on nucleus a, and the promolecule and procrystal are sums over the atoms belonging to the molecule and to the crystal, respectively. The Hirschfeld surface is then defined in a crystal as that region around a molecule where $w(r) \geq \frac{1}{2}$, i.e, the region where the promolecule contribution to the procrystal electron density exceeds that from all other molecules in the crystal.

CHAPTER 3

Computational Methods

All calculations have been performed using Gaussian 09 package (Frisch et al. n.d.). The ground state structure of all molecules have been optimized via density functional theory (DFT) (Hohenberg & Kohn 1964). The structures of emodin and purpurin were optimized using Becke, 3-parameter, Lee-Yang-Parr (B3LYP) functional (Becke 1988, 1992, Cagardová & Lukeš 2017, Lee et al. 1988) and the 6-31++(d,p) basis set. For indigo and alizarin, the molecules were optimized by using B3LYP, Coulomb-attenuating method - B3LYP (CAM-B3LYP) (Yanai et al. 2004) and WB97XD (HalseyMoore et al. 2019) with basis 6-31++G(d,p). The performed calculations include λ for holes and electrons, adiabatic ionization potential (IP), adiabatic electron affinity (EA), chemical hardness (n), HOMO and LUMO energy levels and energy gap E_g.

The excited states of the molecules were determined using time-dependent density functional theory (TD-DFT) (Stratmann et al. 1998) utilizing the functional B3LYP with 6-31++ (d, p) basis set from ground state optimized geometry in vacuum and solvent (Ethanol). This gives the absorption spectra and oscillator strength. The harmonic vibrational frequencies have been performed at the same computational level used for optimization to ensure that all molecules have reached local minima, no negative frequencies have been found.

The reorganization energy for holes (λ_h) and electrons (λ_e) are calculated using the following formula:

$$\lambda_e = (E_0^- - E_-^-) + (E_-^0 - E_0^0)$$

$$\lambda_h = (E_0^+ - E_+^+) + (E_+^0 - E_0^0)$$

where, the $E_0^-(E_0^+)$ is the anionic (cationic) energy of the molecule in optimized neutral structure, the $E_-^-(E_+^+)$ is the anionic (cationic) energy of the molecule in optimized anion (cation) structure, the $E_-^0(E_+^0)$ is the neutral energy of the molecule in optimized anion (cation) structure and the $E_0^0$is the neutral energy of the molecule in optimized neutral structure (Chen et al. 2017, Sahoo et al. 2016, Scharber & Sariciftci 2013).

The ionization potential and electron affinity energies were calculated as per the following equation:

$$IP = E(M^{+}) - E(M^{0})$$

$$EA = E(M^{0}) - E(M^{-})$$

The $E(M^{0})$, $E(M^{+})$ and $E(M^{-})$ are the total energies of the neutral, anionic and cationic state of the molecule (Oshi et al. 2017). The hardness of the molecule, η, was calculated using $(IP - EA)/2$ (Prabha et al. 2017, Sun & Jin 2017).

Furthermore, the intermolecular interaction of emodin and purpurin were investigated to determine the role of these interactions to the crystal lattice through Hirshfeld surface analysis (Spackman et al. 2021b). To aid the interpretation of the interactions, d_{map}, shape index and 2D fingerprint plots (Spackman et al. 2021b) were demonstrated. The 3D energy framework was represented by computing the interaction energies, electrostatic energy, polarization energy, dispersion energy, exchangerepulsion energy, and total intermolecular energy (Jayatilaka & Grimwood 2003) at B3LYP/6-31G (d,p), and a 3.8 Å cluster was generated around the molecule. The calculations were done using the CrystalExplorer17 program (Spackman et al. 2021a). Emodin and hydrated purpurin was used in the representation of the 3D energy framework.

CHAPTER 4

Results and Discussion

4.1 Reorganization Energy

The hole and electron reorganization energies of indigo and it's functionalized molecules are listed in Table 4.1. The λ_h for molecule 6 is lower than the original molecule and it's other functionalized molecules on all basis functionals. Following molecule 6, is the original molecule and then molecule 7 while the other functionalized molecules ranged from 0.208 eV to 0.251 eV using B3LYP, 0.342 1.076 eV at CAM-B3LYP and 0.354 - 0.847 eV at W97XD. The small values of the reorganization energy result in an increase in the charge transfer rate (Chen et al. 2017, Hu et al. 2016, Sun & Jin 2017) and thus expect to improve the V_{OC} and FF (He et al. 2011, Jin & Wang 2015). The λ_h of these molecules is smaller than a commonly used hole transport material, N, N'- Bis (3-methylphenyl)N, N'-diphenylbenzidine (TPD), λ_h = 0.290 eV (Gruhn et al. 2002), which indicates that the hole transport rate for indigo and it's functionalized molecules maybe higher than that of TPD.

The λ_e of indigo is calculated to be 0.175 eV at B3LYP and 0.270 eV at WB97XD which is smaller than all of it's functionalized molecules. Also, the λ_e value of indigo is smaller than a commonly used electron transport material Tris(8-hydroxyquin-olinato) aluminium (Alq_3), λ_e=0.276 eV (Marcus 1964). This implies that indigo may have higher electron transport rate than Alq_3, however, it's functionalized molecules have higher λ_e than that of Alq_3 indicating lower electron transport rate.

The difference between the λ_e and λ_h values for indigo molecule ranges between 0.01 eV and 0.15 eV at all three different functionals and thus may act as a good candidate for ambipolar charge transport material; material which can be used as hole and electron transport (Chen et al. 2017, Sahoo et al. 2016). Adding functional groups plays a role in shifting it to a better hole transport material as all values of λ_h were smaller than λ_e. This suggests that the functionalized molecules of indigo hole carrier mobility is larger than that of electron. Moreover, it also implies that functionalization can be used as good strategy to enhance and tune it's mobility (Menard et al. 2004, Oshi et al. 2017).

The original molecule of alizarin shows smaller values for λ_e than λ_h for all computed functionals by range of 0.120–0.116 eV. Among alizarin and its functionalized molecules, the least λ_h values were in molecule 6 and 7. However, the overall λ_e values for the functionalized molecules are also less than λ_h. Thus, the original alizarin molecule along with its functionalized molecules serves better as electron transport than hole transport. In comparison with indigo, the reorganization energies of indigo are smaller than that of

alizarin. The reorganization energies of hole and electron for alizarin and it's functionalized molecules are listed in Table 4.1. The differences in the values of reorganization energy are also a result of geometry relaxation and contraction during the oxidation and reduction process.

The λ_h and λ_e values of emodin and its functionalized molecules are listed in Table 4.1. For emodin, it can be observed that the λ_h value is smaller than the value of λ_e, 0.22 eV and 0.41 eV, respectively. The λ_h values increased upon introduction of functional groups with the lowest value being 0.38 eV for molecule 4 and 5, and the highest values being 0.40 for molecule 2 and 3. The λ_e showed only slight changes in values with an increase of 0.03 eV on F-functionalized molecule 4 and a decrease on molecule 3 (0.03 eV) and 5 (0.01 eV). The changes in λ_h and λ_e are due to the changes in structure during oxidation and reduction that is attributed to the C-X (functional groups), bonds contribution. As mentioned in section 1.1, the charge transfer rate increases with the decrease of reorganization energy. As such, emodin without functionalization is predicted to have the highest charge transfer rate and serves as a good candidate as a hole transport material and electron transport material upon introduction of functional groups.

Purpurin λ_h and λ_e values are also listed in Table 4.1. Unlike emodin, the value of λ_e is smaller than λ_h value, 0.39 eV and 0.59 eV, respectively. Accordingly, purpurin without functionalization may act as good electron transport material. The addition of functional groups has led into minor decrease of λ_h in molecules 2, 3, 5 and 6 with λ_h values of 0.56, 0.56, 0.58, 0.58 eV, respectively. The only increase was in Cl-functionalized molecule 4 with λ_h to be 0.60 eV. The changes in λ_e values are also minor, with the largest increase for molecule 2 and 6 by 0.03 eV and the smallest decrease for molecule 3 by 0.02 eV. While no change occurred in Cl-functionalized molecules, 4 and 5. Based on the given data, purpurin is inclined to have high charge transport rate as an electron transport material and its functionalized molecules may also have similar charge transfer rate as electron transport materials. In general, for halogenated molecules, the values for F show higher reorganization energy than Cl, in emodin and purpurin as a result of higher electronegativity of Fluorine. This is in agreement with results of halogenated naphthalene (Oshi et al. 2017) and tetracene (Sancho-García et al. 2010). It is suggested that the intra-ring functionalization of molecules may yield better results in minimizing the reorganization energy as it avoids the introduction of additional degrees of freedom for geometric relaxation (Li et al. 2012). Overall, the values of λ_h and λ_e are similar to those of proposed organic semiconductors (Li et al. 2012, Oshi et al. 2017, 2018, 2019).

The values of chemical hardness for the molecules are also presented in Table 4.1. The chemical hardness (η) is defined as the resistance of the chemical potential to change in the number of electrons (Sun & Jin 2017), the functionalized molecules show similar values of η to that emodin and purpurin, indicating their stability.

	B3LYP				CAM-B3LYP				WB97XD			
Molecule	λ_h	λ_e	IP	EA	λ_h	λ_e	IP	EA	λ_h	λ_e	IP	EA
Indigo												
1 – None	0.195	0.175	6.968	1.906	0.331	0.477	7.060	1.894	-0.171	-0.270	6.539	1.826
2 – (2)NO_2	0.223	0.295	7.736	3.072	1.076	0.266	7.875	2.133	0.467	0.472	8.297	2.819
3 – CN	0.208	0.293	7.631	2.785	0.342	0.443	7.758	2.728	0.354	0.449	7.752	2.675
4 – (8)F	0.251	0.411	7.778	2.762	0.376	0.523	7.932	2.774	0.383	0.528	7.875	2.682
5 – (4)F	0.235	0.409	7.429	2.368	0.543	0.525	7.550	2.369	0.847	0.824	7.516	2.291
6 – (8)Cl	0.189	0.342	7.485	2.80	0.326	0.457	7.685	2.804	0.340	0.817	7.683	2.761
7 – (4)Cl	0.199	0.360	7.339	2.511	0.339	0.478	7.489	2.509	0.353	0.484	7.486	2.459
Alizarin												
1 – None	0.482	0.366	8.236	1.622	0.632	0.492	8.127	1.939	0.603	0.483	8.112	1.860
2 – (4)Cl	0.365	0.478	8.235	2.002	0.646	0.532	8.243	2.454	0.636	0.555	8.259	2.360
3 – (2)Cl	0.399	0.395	8.278	1.925	0.638	0.495	8.309	2.290	0.613	0.487	8.295	2.218
4 – (2)F	0.495	0.408	8.321	1.845	0.632	0.526	8.347	2.224	0.609	0.517	8.320	2.133
5 – (4)F	0.345	0.436	8.811	1.992	0.636	0.555	8.403	2.396	0.614	0.544	8.369	2.293
6 – (2)CN	0.346	0.319	9.071	2.562	0.607	0.456	8.658	2.897	0.587	0.451	8.642	2.825
7 – (4)CN	0.369	0.686	9.355	4.057	0.608	0.454	8.955	3.503	0.593	0.449	8.938	3.438
8 - (2)NO_2	0.511	0.376	8.446	2.290	0.621	0.490	8.458	2.526	0.601	0.490	8.438	2.439

Table 4.1: λ_h and λ_e, IP and EA (in eV) and η of Indigo and Alizarin and their functionalized molecules calculated at B3LYP/6-31++G (d,p),CAM-B3LYP/6-31++G (d,p),WB97XD/6-31++G (d,p) level of theory

Molecule	λ_h	λ_e	IP	EA	n
Emodin					
1 – None	0.22	0.41	8.74	1.85	3.44
2 – (1) Ethylene	0.40	0.41	8.13	1.87	3.13
3 – (1) CN	0.40	0.38	8.42	2.33	3.05
4 – (1) F	0.38	0.43	8.24	1.98	3.13
5 – (1) Cl	0.38	0.40	8.30	2.13	3.09
Purpurin					
1 – None	0.59	0.39	8.43	1.85	3.29
2 – (1) NO_2	0.56	0.42	8.06	2.59	2.74
3 – (1) CN	0.56	0.37	8.01	2.37	2.82
4 – (1) Cl	0.60	0.39	7.81	2.04	2.88
5 – (2) Cl	0.58	0.39	7.88	2.19	2.85
6 – (2) F	0.58	0.42	7.93	2.12	2.91

Table 4.2: λ_h and λ_e, IP and EA (in eV) and η of Emodin and Purpurin and their functionalized molecules calculated at B3LYP/6-31++G (d,p) level of theory

4.2 Ionization and Electron Affinity

The values of IP and EA of indigo and it's functionalized molecules are given in Table 4.1. The values of IP of all molecules increase with the addition of functional groups, indigo molecule shows the least IP value while the 8 F functionalized molecule shows the highest value. This indicates that the addition of more electronegative functional shifts the molecule to a better n-type semiconductor, as n-type semi-conductors are known to have higher IP values (Louis et al. 2017). The IP of indigo functionalized molecules with electronegative atoms, O and N is expected to be high, the addition of functional groups with higher electronegativity results in higher IP values. Thus, F^- functionalized molecule is of the higher IP than the Cl^- functionalized molecule which means that the F^- functionalized molecule can act as better n-type semi-conductor than Cl functionalized which is in agreement with halogen functionalization of naphthalene (Oshi et al. 2017). The addition of further F and Cl functional atoms in molecule 4 and 6, also contributes to higher IP values. The functional groups that were added to the molecule are considered

as de-activators and withdraws electron from the ring, the descending order of the de-activators is NO2 > CN > Cl > F (McMurry & Simanek 2008). Thus, the EA is expected to decrease with the addition of these substituents, respectively. This agrees with the values in Table 4.1. The IP for functionalized alizarin shows the highest values in CN functionalized molecules, 6 and 7, with values of 9.071 eV (B3LYP), 8.658 eV (CAM-B3LYP),8.642 eV (WB97XD) and 9.355 eV (B3LYP),8.955 eV (CAM-B3LYP), 8.938 eV (WB97XD) respectively. While Cl functionalized molecules, 2 and 3, represents the least values of 8.235 eV (B3LYP), 8.243 eV (CAM-B3LYP), 8.259 eV (WB97XD) and 8.278 eV (B3LYP), 8.309 eV (CAM-B3LYP), 8.295 eV (WB97XD), respectively. For the EA of functionalized alizarin, the functionalization with the highly activating group, i.e., F group has the lowest EA with value of 1.845 eV (B3LYP), 2.224 eV(CAM-B3LYP) and 2.133 eV (WB97XD) in molecule 4. The highest EA is calculated for CN functionalized molecules,7 and 6. Molecule 7 with highest values of 4.057 eV (B3LYP), 3.508 eV (CAM-B3LYP) and 3.438 eV (WB97XD). These values are attributed to the deactivating property of cyanide group making the molecules n-type characteristics (Louis et al. 2017).

In comparison with indigo, alizarin and its functionalized molecules show overall lower values of electron affinity. The values of IP and EA of alizarin and it's functionalized molecules are given in Table 4.1.

The values IP and EA for emodin, purpurin, and their functionalized molecules are illustrated in Table 4.1. One of the concerns in n-type organic semiconductor systems is the lack of stability of their radical anions in the air (De Leeuw et al. 1997) and functionalization of molecules may be used to tune IP and EA values for a more stabilized molecule. The IP value of emodin is calculated to be 8.74 eV and the EA is 1.85 eV, and because of the similarity in structure, the IP and EA of purpurin have shown similar values to that of emodin with values of 8.43 eV and 1.85 eV, respectively. The functionalization of emodin and purpurin results in a decrease of IP and an increase in EA values. The values of emodin IP are in the sequence of molecules 1 > 3 > 5 > 4 > 2 and for EA values

3 > 5 > 4 > 2 > 1 and for purpurin the IP values are in the sequence of 1 > 2 > 3 > 6 > 5 > 4 and for EA 2 > 3 > 5 > 6 > 4 > 1. The NO_2-functionalized purpurin has the highest IP and EA values due to the negative resonance effect and electron affinity of the NO_2 group. Electrons are withdrawn from the rings, leading to electron deficit at all positions of the fused rings. It is followed by the CN-functionalized molecule, which is attributed to the interactions of the nitrogen lone pair of electrons (negative resonance effect) with the p-electron clouds of the fused rings, as well as the inductive effect of the electronegative nitrogen atom. These results are in agreement with the NO_2 and CN functionalization of tetracene (Oshi et al. 2018).

Similarly, the CN-functionalized molecule in emodin has the highest EA value, 2.33 eV. The 2Cl-functionalized purpurin molecule has a higher EA value than the 2F-functionalized molecule,that is accounted for by the higher ability of Cl to withdraw electrons,taking into consideration resonance and inductive effects. This is in agreement with halogenated pentacene (Kuo et al. 2007) and naphthalene (Oshi et al. 2017). In addition, the Cl-functionalized emodin molecule also has a higher EA than the F-functionalized molecule.

4.3 HOMO and LUMO Energy and Optical Properties

In indigo, the HOMO values are in the order of molecule 1> 5> 7> 6> 3> 2> 8 and for LUMO 1> 5> 7> 6> 3> 4> 2. Therefore, the values of E_g is in the sequence of 5> 4> 1> 7> 6> 3> 2, the values of E_g for all functionalized molecules are less than the non-functionalized molecule except for molecule 4 and 5. The least value of E_g is computed for molecule 2 with 2.24 eV which is also expected to reflect on improved I_{SC} (Jin & Wang 2015). In general, the Cl functionalized molecules show lower gap than the F-functionalized molecules, followed by CN with value of 2.372 eV. The results are consistent with the IP and EA, it also indicates that addition of functional groups can lead to the alternation in the molecular properties. The values of E_g, HOMO and LUMO of indigo and it's functionalized molecules are reported in Table 4.3.

Molecule	E_g(eV)	λ_{abs}	HOMO(eV)	LUMO(eV)	*f*
Indigo					
1 – None	2.462	551.48	-5.63	-3.16	0.2767
2 – (2)NO_2	2.240	608.1	-6.46	-4.22	0.2805
3 – (2)CN	2.372	568.42	-6.36	-3.98	0.3262
4 – (8)F	2.471	548.47	-6.48	-4.01	0.3248
5 – (4)F	2.490	547.23	-6.10	-3.62	0.2427
6 – (8)Cl	2.416	1253.38	-6.34	-3.92	0
7 – (4)Cl	2.433	563.27	-6.11	-3.68	0.3024
Alizarin					
1 – None	3.73	431.34	-6.72	-2.99	0
2 – (4)Cl	3.61	429.44	-6.83	-3.22	0.0134
3 – (2)Cl	3.59	430.03	-6.82	-3.23	0
4 – (2)F	3.61	426.17	-6.82	-3.21	0
5 – (4)F	3.55	435.29	-6.89	-3.34	0.0013
6 – (2)CN	3.32	446.75	-7.17	-3.85	0
7 – (4)CN	3.11	474.28	-7.50	-4.39	0
8 - (1)NO_2	3.38	472.38	-6.95	-3.58	0.0033
Emodin					
1 – None	3.52	413.28	-6.69	-3.18	0.1139
2 – (1) Ethylene	3.51	414.72	-6.69	-3.18	0.1173
3 – (1)CN	3.40	427.31	-7.01	-3.62	0.091
4 – (1)F	3.51	411.77	-6.81	-3.30	0.1063
5 – (1)Cl	3.45	421.43	-6.89	-3.44	0.1183
Purpurin					
1 – None	3.12	452.09	-6.31	-3.19	0.1274
2 – (1)NO_2	2.84	509.51	-6.68	-3.84	0.0797
3 – (1)CN	2.97	480.52	-6.63	-3.66	0.1138
4 – (1)Cl	3.09	455.57	-6.44	-3.35	0.1349
5 – (2)Cl	3.06	461.24	-6.53	-3.47	0.135
6 – (2)F	3.09	456.44	-6.54	-3.45	0.1241

Table 4.3: HOMO-LUMO Gap of Indigo, Alizarin and derivatives

The HOMO and LUMO values of alizarin and it's functionalized molecules is in the sequence of 1> 4= 3> 2> 5> 8> 6> 7> and 1> 4> 2> 3> 5> 8> 6> 7, respectively. The E_g in alizarin is in the order of 1> 2= 4> 3> 5> 8> 6> 7, the E_g value of alizarin molecule is higher than indigo by a 1.268 eV due to the presence of 2 oxygen and nitrogen elements, the overall substituted molecules of alizarin are also higher than indigo functionalized molecules. The highest E_g in the functionalized molecules is in molecule 2 and molecule 4 with value of 3.61 eV and the smallest value is in molecule 7 with value of 3.11 eV. In general, the energy gaps of both indigo and alizarin along with their functionalized

molecules fall between the approximate energy gaps of organic semi-conductors, i.e. between 1.4 - 4.2 eV (Chen et al. 2017). The LUMO values of both molecules were lowered upon the introduction of the functional groups which denotes higher ability to accept electrons (Prabha et al. 2017) and these values are in agreement with increasing IP and EA reported values in Table 4.1.The typical range of p-type semi-conductors for HOMO is 4.9–5.5 eV, while n-type semi-conductors LUMO energy levels falls between 3.0 and 4.0 eV (Cardia et al. 2014). The LUMO values of indigo and alizarin falls along with its functionalized molecules fall within the range of n-type semi-conductors, with the exception of molecule 2 and 4 in indigo and molecule 7 in alizarin. However, higher charge mobility is expected to be in indigo than in alizarin due to it's smaller energy gap (Oshi et al. 2017). The values of E_g, HOMO and LUMO of alizarin and it's derivatives are reported in Table 4.3.

The HOMO and LUMO qualitative molecular representations of indigo and alizarin and their functionalized molecule in S_0 are depicted in figure 3 and 4, respectively. For Indigo, the HOMO and LUMO is delocalized on the molecule and it's derivative, except for some of the functional groups, the transition is within the benzene ring mainly. This indicates a strong overlap between the HOMO and LUMO that leads to strong optical absorption due to electron excitation $S_0 \rightarrow S_1$ which can be assigned as HOMO and LUMO transition. In figure 4.1, the delocalization predicts the transition from the oxygen substituted rings to the benzene ring. The study of these frontier molecular orbital (FMO), in qualitative manner, is insightful in predicting the electron transition (Sun & Jin 2017).

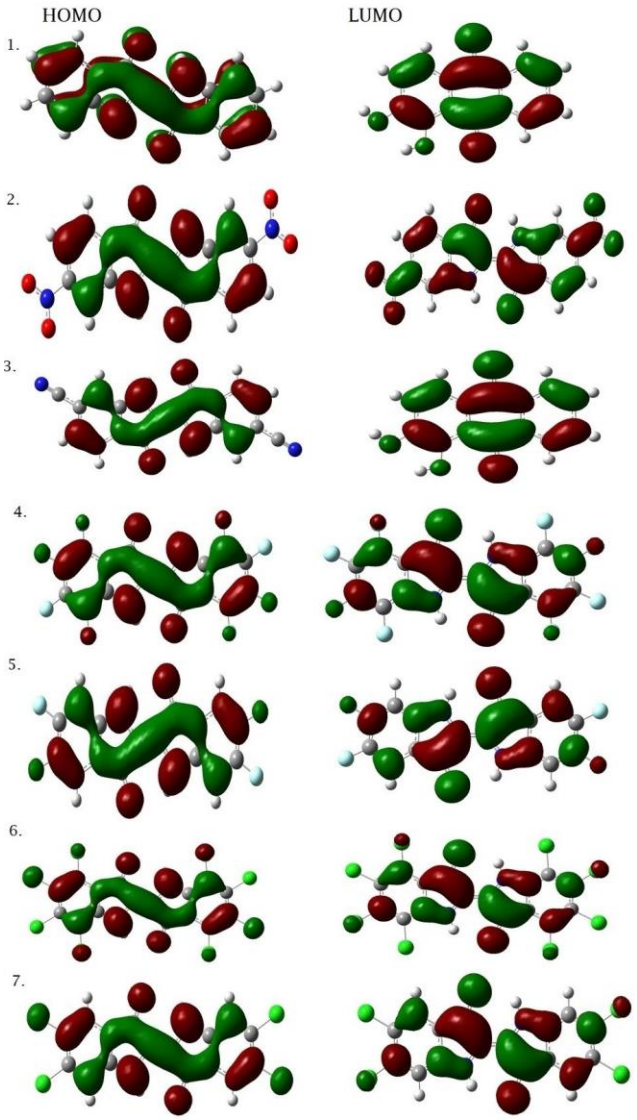

Fig. 4.1. HOMO and LUMO of Indigo molecule 1 - 7

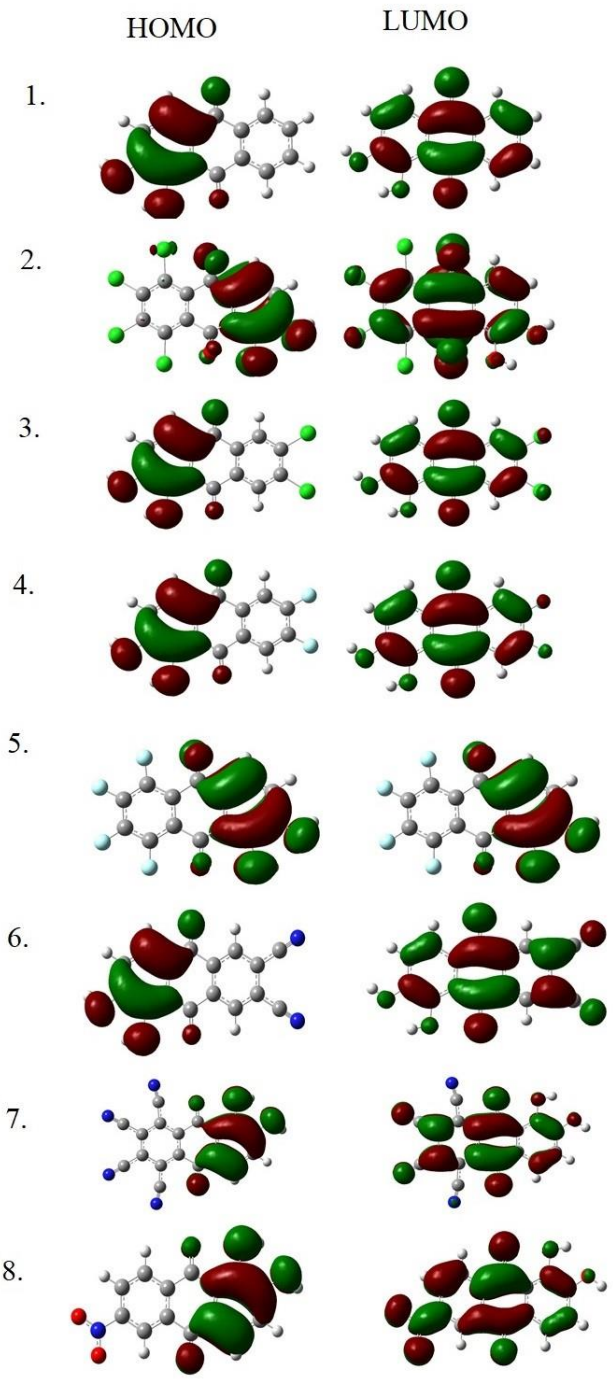

Fig. 4.2. HOMO and LUMO of Alizarin molecule 1 – 8

The oscillator strength of the Indigo and Alizarin and their derivatives is shown in Table 4.3. The oscillator strength expresses the probability of absorption of electromagnetic radiation, larger oscillator strength represents larger absorption coefficient. In further investigation, indigo excited state S_1 corresponds to the strongest absorption at 551.48 nm (f= 0.2767) and 596.75 nm (f= 0.3500) in vacuum and solvent, respectively. As for it's functionalized molecules, molecule 2 strongest absorption was 608.10 nm (f= 0.2805) and 681.57 nm (f= 0.3384)at excited state S_1 in vacuum and solvent, respectively, molecule 3 strongest absorption was 568.42 nm (f= 0.3262) and 620.36 nm (f= 0.4075) at excited state S_1 in vacuum and solvent, respectively, molecule 4 showed strongest absorption in 548.47 nm (f= 0.3248) and 588.55 nm (f= 0.3996) at excited state S_1 in vacuum and solvent, respectively, molecule 5 strongest absorption was 547.23 nm (f= 0.2427) and 586.79 nm (f= 0.3171) at excited state S_1 in vacuum and solvent, respectively. While molecule 6 strongest absorption in vacuum was 576.92 nm (f= 0.4156) at excited state S_2, the solvent absorption was 608.17 nm (f= 0.4543) at excited state S_1. The strongest absorption in molecule 7 was 563.27 nm (f= 0.3024) and 602.83 nm (f= 0.3907) excited state S_1 in vacuum and solvent, respectively. The strongest absorption was noted in indigo 8Cl functionalized, molecule 6. While, the other excited states of indigo and it's functionalized molecules can be considered as negligible due to the low values of oscillator strength as shown in 4.3.

In Alizarin, the original molecule excited state S_3 corresponds to the strongest absorption at 381.58 nm (f= 0.1036) in vacuum and excited state S_2 at 407.63 nm (f= 0.1750) in solvent. For the functionalized molecules, molecule 2 strongest absorption was 429.30 nm (f= 0.1273) in solvent at S_1, molecule 3 strongest absorption was 394.82 nm (f= 0.1314) in vacuum at S_2 and 418.92 nm (f= 0.1825) in solvent at S_1, molecule 4 strongest absorption was 391.60 nm (f= 0.1209) in vacuum and 414.88 nm (f= 0.1697) in solvent at S_2, molecule 5 strongest absorption was 427.23 nm (f= 0.1513) in solvent at S_1, molecule 6 was 620.36 nm (f= 0.4075) in solvent at S_1, molecule 7 was 507.70 nm (f= 0.1172) in solvent at S_1 and molecule 8 was 461.59 nm (f= 0.0759) in solvent at S_1. The highest absorption among alizarin and it's functionalized molecules was 2Cl, molecule 3, however, alizarin absorption strength is relatively lower than that of indigo. The overall

λ_{max} values are in agreement with the reported E_g of the molecules in which the smaller E_g resulted in higher λ_{max}. The maximum absorptions for indigo and alizarin at different excitation states along with their transition energies are in Table 4.4, in vacuum and chloroform. In the presence of solvent, the neat and functionalized molecules have shown a redshift absorption in different excitation states as illustrated also in Table 4.4 and the absorption strength seen in solvent was stronger than in vacuum, which means that the solvent have effects on the absorption of the molecules to light.

The stability of the molecules was predicted using hardness which describes the resistance of the chemical potential to change in the number of electrons (Sun & Jin 2017). The η values, listed in Table 4.1, of the substituted molecules are similar to those of the indigo and alizarin which indicates that the functionalized molecules are also stable.

The values of E_g, HOMO and LUMO of emodin, purpurin and their functionalized molecules are shown in Table 4.3, the molecules E_g falls within the range of organic semiconductors, 1.4 - 4.2 eV (Chen et al. 2017). The functionalization of emodin and purpurin contributed in lowering the energy gap that predicts kinetic stability and an increase in conductivity.

The energy gap of emodin and its functionalized molecules ranged between 3.40 - 3.52 eV, the smallest E_g value was for CN-functionalized molecule 3, 3.40 eV and followed by Cl-functionalized molecule 5, 3.45 eV and accordingly is predicted to have better conductivity. In addition, the LUMO energy levels and λ_e of CN and Cl-functionalized molecules also have the lowest values which results in improving emodin functionality as n-type material.

The overall LUMO values decreased except for C_2H_2, the LUMO values ordered as molecule 1= 2> 4> 5> 3. The CN-functionalized molecule showed the lowest value leading into smallest energy gap value. The HOMO levels also decreased in value with the order of molecule 1= 2> 4> 5> 3.

The HOMO and LUMO values of purpurin and its functionalized molecules are in the sequence of molecule 1> 4> 5> 6> 3> 2 and 1> 4> 6> 5> 3> 2, respectively. The E_g values range from 2.84 - 3.12 eV, emodin showed the highest E_g value of 3.12 eV with NO_2-functionalization the value decreased into 2.84 eV to become the smallest E_g among the molecules, followed by CN-functionalized molecule 3.

The decrease of E_g of emodin and purpurin upon addition of functional groups is in accordance with the results obtained for functionalization of anthracene and tetracene by F, Cl, NO_2 and CN (Oshi et al. 2018). Overall, the LUMO values of the molecules is in the range of typical n-type materials between -3.0 and -4.0 eV, lowering of LUMO also results in increase of stability (Li et al. 2012) and higher ability to accept electrons (Prabha et al. 2017). Hence, the studied molecules are proposed to be good n-type materials.

The oscillator strength of emodin and purpurin and their functionalized molecules is presented in Table 4.4. Oscillator strength express the probability of absorption of electromagnetic radiation, the higher the oscillator strength is for a molecule the higher expected absorption. In further studies, the strongest absorption for emodin corresponds to excited state S_1 with value of 413.28 nm (f = 0.1139) in vacuum. For molecule 2, the strongest absorption was at excited state S_1 with value of 429.11 nm (f = 0.1427) in solvent. The strongest absorption in molecule 3 corresponds to 439.71 nm (f = 0.1168) in solvent at excited state S_1. The excited state S_1 shows the strongest absorption for molecule 4 with value of 425.47 nm (f = 0.1283) in solvent. Finally, molecule 5 also shows strongest absorption at excited state S_1 with value of 434.66 nm (f = 0.146) in solvent.

For purpurin, the excited state S_1 corresponds to the strongest absorption with values of 461.81 nm (f = 0.194) in solvent. For NO_2- functionalized molecule the strongest absorption value is 541.1 nm (f = 0.0944) in solvent at excited state S_1. For molecules 3, 1022.69 nm (f = 0.297) in solvent at excited state S_1. For the 1Cl-functionalized molecule at excited state S_1 with value of 466.58 nm (f = 0.2031) in solvent. As for the 2Cl-functionalized molecule which also corresponds to excited state S_1 with value of 473.32 nm (f = 0.2028) in solvent. For molecule 6, the strongest absorption takes place in vacuum with value of 456.44 nm (f = 0.1241). It can be noticed from the give values in Table 4.4, that the solvent resulted in red shift of the maximum absorption. Moreover, the decrease of the E_g values also resulted in a red shift in the maximum absorption as listed in Table 4.3.

	Excited State 1				Excited State 2				Excited State 3			
Molecule	λ_{max}(nm) f		λ_{max}(nm) f		λ_{max}(nm) f		λ_{max}(nm) f		λ_{max}(nm) f		λ_{max}(nm) f	
Emodin	Without Solvent		With Solvent		Without Solvent		With Solvent		Without Solvent		With Solvent	
Indigo												
1 – None	551.48	0.2767	596.75	0.3500	458.03	0	476.67	0	433.44	0	426.84	0
2 – (2)NO_2	608.1	0.2805	681.57	0.3384	479.35	0	532.01	0	466.55	0	487.57	0
3 – (2)CN	568.42	0.3262	620.36	0.4075	457.24	0	473.14	0	447.15	0	443.52	0
4 – (8)F	548.47	0.3248	588.55	0.3996	451.41	0	462.81	0	424.71	0	417.69	0
5 – (4)F	547.23	0.2427	586.79	0.3171	469.11	0	481.35	0	428.75	0	423.54	0
6 – (8)Cl	1253.88	0	608.17	0.4543	576.92	0.4156	485.89	0	519.65	0	430.23	0
7 – (4)Cl	563.27	0.3024	602.83	0.3907	481.38	0	490.8	0	432.47	0	427.64	0
Alizarin												
1 – None	431.34	0	419.83	0	388.39	0	407.63	0.175	381.58	0.1036	380.18	0
2 – (4)Cl	429.44	0.0134	429.3	0.1273	400.99	0.0709	408.46	0.0341	383.42	0.0551	378.81	0.0242
3 – (2)Cl	430.03	0	418.92	0.1825	394.82	0.1314	418.92	0.0001	385.27	0	379.58	0
4 – (2)F	426.17	0	415.16	0.0001	391.6	0.1209	414.88	0.1697	382.94	0	377.44	0
5 – (4)F	435.29	0.0013	427.23	0.1513	403.71	0.0962	420.57	0.0146	391.01	0.0221	384.32	0.005
6 – (2)CN	446.75	0	620.36	0.4075	430.85	0.1035	473.14	0	398.95	0	443.52	0
7 – (4)CN	474.28	0	507.7	0.1172	465.27	0.0927	471.62	0.0195	424.77	0.0051	458.73	0
8 - (1)NO_2	472.38	0.0033	461.59	0.0759	406.84	0.0497	438.47	0	396.47	0.0001	389.46	0
Emodin												
1 – None	413.28	0.1139	419.83	0	388.39	0	407.63	0.175	381.58	0.1036	380.18	0
2 – (1) Ethylene	414.72	0.1173	429.11	0.1427	413.11	0.0003	403.01	0	365.56	0.012	378.55	0.0356
3 – (1) CN	427.31	0.091	439.71	0.1168	417.29	0	408	0	362	0	386.1	0.039
4 – (1) F	411.77	0.1063	425.47	0.1283	409.61	0	399.56	0	356.28	0	380.94	0.0464
5 – (1) Cl	421.43	0.1183	434.66	0.146	412.82	0	402.54	0	360.14	0	383.27	0.026
Purpurin												
1 – None	452.09	0.1274	461.81	0.194	449.76	0	425.89	0	350.37	0	370.06	0.0317
2 – (1) NO_2	509.51	0.0797	541.1	0.0944	467.25	0	442.21	0	374.59	0.0096	401.81	0.0597
3 – (1) CN	480.52	0.1138	1022.69	0.0297	457.45	0	1011.86	0.001	357.24	0	693.33	0
4 – (1) Cl	455.57	0.1349	466.58	0.2031	446.72	0	423.55	0	366.79	0.0651	379.2	0.0608
5 – (2) Cl	461.24	0.135	473.32	0.2028	447.96	0	424.82	0	373.14	0.0318	382.31	0.0322
6 - (2) F	456.44	0.1241	708.01	0	444.04	0	478.79	0	365.57	0.0265	465.55	0

Table 4.4: Maximum absorption and oscillator strength of Emodin and Purpurin along with their derivatives in presence and absence of ethanol solvent

4.4 Hirschfeld surface analysis

The Hirschfeld surface analysis aids in the quantification and visualization of intermolecular interactions by utilizing different colors and intensities in graphical representation. Hirschfeld surface analysis has been used to investigate various intermolecular interactions in the crystal structure of organic molecules and complexes (Al-Resayes et al. 2020, Van Thong et al. 2022). The d_{norm} (normalized contact distance) maps of emodin and purpurin are depicted in Fig.4.3. The contacts with shorter distances (close contacts) than the Van der Waals radii are represented by red surfaces, while the blue surfaces represent contacts with longer distances (distance contact). The white surfaces denote distance equivalent to the sum of Van der Waals radii. The red regions in emodin and purpurin appears to originate from the –OH groups in the molecules. The red regions of the molecules may act as donors in intermolecular reactions. Thereby, it is expected that their functionalized molecules with electronegative groups would adhere more sites that act as donors. The shape-index of emodin and purpurin on the Hirshfeld surface is presented in Fig. 4.4. The red and blue regions represent the donor and acceptor groups of the molecule, the adjacent red and blue triangles denote p-p stacking interaction among the structures. The 2D fingerprint plots and fragment patches of emodin and purpurin are illustrated in Figs. 4.5 and 4.6, respectively. The de and di on the plots represent the distances to the nearest atom center, external and internal to the surface. Points on the plot without contribution are gray colored and points with small contribution is blue colored through green to red for the points with the largest contribution. The most significant interaction in emodin is O-H/H- -O that contributes 31.8% to the overall surface. The second largest interaction is H–H with contribution of 30.1% as pair wings, followed by C- -H/H- -C (15.9%), C- -C (10.9%) and O- -C/C-O (9.1%).

In purpurin, the O- -H/H- -O interactions dominated with a contribution of 41%, while the H- -H and C- -C interactions were 26.6% and 22.3%, respectively. Both molecules have other small contributions; emodin O- -O (2.2%) and purpurin C- -H/H- -C (5.5%), O- -O (2.8%) and C- -O/O- -C

(1.9%).

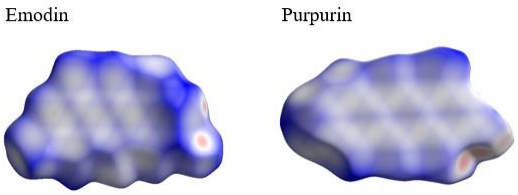

Fig. 4.3: Hirschfeld surface of emodin and purpurin plotted over dnorm in the range of -0.4160 to 1.2106 and -1.7662 to 0.8459 a.u, respectively

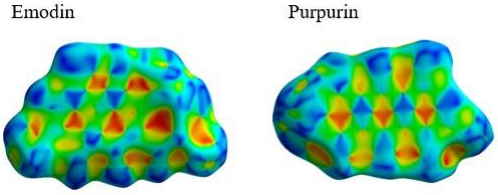

Fig. 4.4. Shape-index of emodin and purpurin on Hirschfeld surface

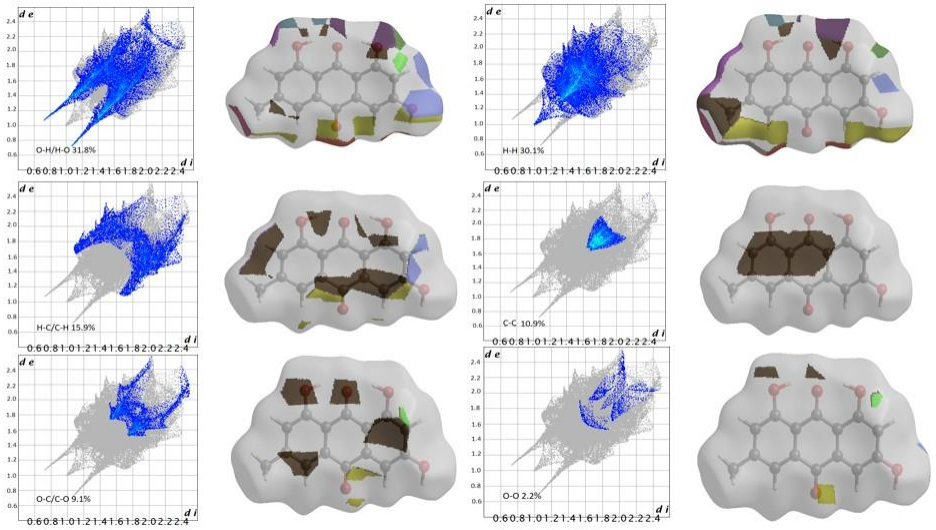

Fig. 4.5. Emodin two-dimensional fingerprint plots and fragment patches (surface patches adjacent to neighboring surfaces are colored separately) for intermolecular interactions.

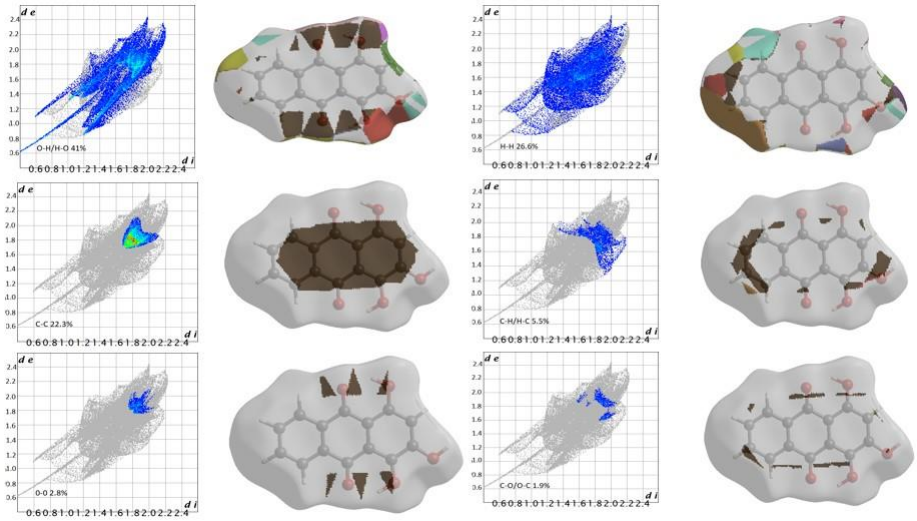

Fig. 4.6. Purpurin two-dimensional fingerprint plots and fragment patches (surface patches adjacent to neighboring surfaces are colored separately) for intermolecular interactions.

4.5 Energy Frameworks

The calculated interaction energies energy E_{tot} (kJ mol^{-1}) namely, electrostatic (E_{elec}), polarization (E_{pol}), dispersion (E_{dis}), exchange-repulsion (E_{rep}) are used to generate 3D representation of the major interactions in the form of energy frameworks, Fig.4.7. The interaction energies relative strength in individual directions are represented by exhibited cylinder-shaped energy frameworks, the size of the interactions that are less than 5 kJ mol^{-1} have been excluded. It can be seen that the intermolecular interactions are dominated by dispersion forces in emodin and purpurin, Fig 4.7.

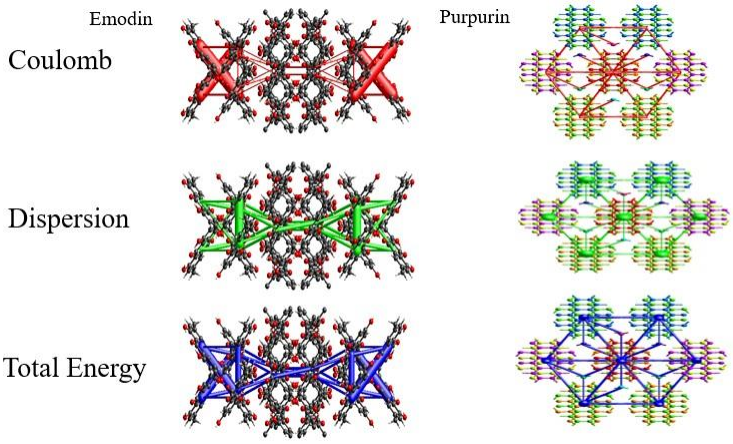

Fig. 4.7. Emodin and Purpurin energy framework, coulomb energy (red), dispersion energy (green) and total energy (blue)

CHAPTER 5

Conclusion

The optical and electronic properties of four organic molecules, Indigo, Alizarin, Emodin and Purpurin were investigated. The reorganization energy, ionization potential, electron affinity, the frontier molecular orbitals, the energy gaps and were calculated by DFT. The maximum absorptions, oscillator strength in vacuum and solvent were calculated by TD-DFT methods. Those calculations were carried out to understand the electronic and optical properties of the material, the effect of electronegative substituents on those properties and the potential use of the neat and substituted molecules.

It was found that Indigo and Alizarin, along with their derivatives, have the potential to be used as OPV due to their acceptable reorganization energy values that reflects that those molecules can have high charge mobility when used as solar cell. The energy gap of those molecules ranged within the typical organic semiconductor, 1.4–4.2 eV and the absorption range was within the visible spectrum range.

In emodin and purpurin, there was an overall increase in reorganization energy due to the geometrical changes of the molecule upon oxidation and reduction processes. However, the decrease in Eg and LUMO energy levels of the molecules pre-predicts the increase in stability and conductivity. Furthermore, an increase in EA values was also noted to reinforce the molecule's ability to accept electrons. Hence, the functionalization of emodin and purpurin strengthened the n-type properties of the molecules. The energy gaps of the molecules are within the range of semiconductors (1.4–4.2 eV) and the absorption ranges of the molecules are within the visible range. Based on the given data, we have concluded that emodin and purpurin along with their functionalized molecules are good candidates for organic semi-conductors. Also, the intermolecular interactions and 3D energy framework of emodin and purpurin molecules were studied through Hirshfeld surface analysis. It has been shown that the main interaction in the crystal structure of emodin and purpurin is O–H/H–O and dispersion energy was dominant in the 3D energy framework.

The addition of the electronegative substituents also plays an important role in modifying molecular properties in which some molecules maybe converted from n-type to p-type due to optical and electronic property changes. It is important to carry out theoretical studies of potential molecules to understand the optical and electronic properties of the molecules and have a better design of OPV with higher efficiency.

6 REFERENCES

(**n.d.a**). National Center for Biotechnology Information. PubChem Compound Database, accessed July 02, 2021, https://pubchem.ncbi.nlm.nih.gov/compound/Indigo.

(**n.d.b**).Alizarin (CHEBI:16866), accessed Jul. 02.2022,
https://www.ebi.ac.uk/chebi/searchId.do?chebiId = CHEBI
(**n.d.c).** National Center for Biotechnology Information. PubChem Compound Database accessed Jul 02,2021,https://pubchem.ncbi.nlm.nih.gov/compound/Emodin.

(**n.d.d**). National Center for Biotechnology Information. PubChem Compound Database accessed Jul 02,2021, https://pubchem.ncbi.nlm.nih.gov/compound/Purpurin.

Al-Resayes, S. I., Azam, M., Trzesowska-Kruszynska, A., Kruszynski, R., Soliman, S. M., Mohapatra, R. K. & Khan, Z. (2020). Structural and theoretical investigations, hirshfeld surface analyses, and cytotoxicity of a naphthalene-based chiral compound, *ACS omega* **5**(42): 27227–27234.

Arbouch, I., Karzazi, Y. & Hammouti, B. (2014). Organic photovoltaic cells: operating principles, recent developments and current challenges–review, *Physical and Chemical News* **72**: 73–84.

Atkins, P. & De Paula, J. (2006). Atkins' physical chemistry 8th edition.

Aubouy, L., Gerbier, P., Guérin, C., Huby, N., Hirsch, L. & Vignau, L. (2007). Study of the influence of the molecular organization on single-layer oleds' performances, *Synthetic metals* **157**(2-3): 91–97.

Bagher, A. M., Vahid, M. M. A. & Mohsen, M. (2015). Types of solar cells and application, *American Journal of optics and Photonics* **3**(5): 94–113.

Bao, Z., Lovinger, A. J. & Brown, J. (1998). New air-stable n-channel organic thin film transistors, *Journal of the American Chemical Society* **120**(1): 207–208.

Becke, A. D. (1988). Density-functional exchange-energy approximation with correct asymptotic behavior, *Physical review A* **38**(6): 3098.

Becke, A. D. (1992). Density-functional thermochemistry. i. the effect of the exchange-only gradient correction, *The Journal of chemical physics* **96**(3): 2155–2160.

Becquerel, A. (1839). Mémoire sur les effets électriques produits sous l'influence des rayons solaires, *Compt. Rend. Acad. Sci* **9**: 561–567.

Bernede, J. (2008). Organic photovoltaic cells: history, principle and techniques, *Journal of the Chilean Chemical Society* **53**(3): 1549–1564.

Borsenberger, P. M. & Weiss, D. S. (1993). *Organic photoreceptors for imaging systems*, Vol. 39, M.
Dekker New York.

Brédas, J.-L., Calbert, J. P., da Silva Filho, D. & Cornil, J. (2002). Organic semiconductors: A theoretical characterization of the basic parameters governing charge transport, *Proceedings of the National Academy of Sciences* **99**(9): 5804–5809.

Cagardová, D. & Lukeš, V. (2017). Molecular orbital analysis of selected organic p-type and n-type conducting small molecules, *Acta Chimica Slovaca* **10**(1): 6–16.

Cardia, R., Malloci, G., Mattoni, A. & Cappellini, G. (2014). Effects of tips-functionalization and perhalogenation on the electronic, optical, and transport properties of angular and compact dibenzochrysene, *The Journal of Physical Chemistry A* **118**(28): 5170–5177.

Chapin, D. M., Fuller, C. & Pearson, G. (1954). A new silicon p-n junction photocell for converting solar radiation into electrical power, *Journal of Applied Physics* **25**(5): 676–677.

Chen, H.-Y. & Chao, I. (2006). Toward the rational design of functionalized pentacenes: reduction of the impact of functionalization on the reorganization energy, *ChemPhysChem* **7**(9): 2003–2007.

Chen, Z., He, Z., Xu, Y. & Yu, W. (2017). Density functional theory calculations of charge transport properties of 'plate-like'coronene topological structures, *Journal of Chemical Sciences* **129**(9): 1341–1347.

Chesterfield, R. J., Newman, C. R., Pappenfus, T. M., Ewbank, P. C., Haukaas, M. H., Mann, K. R., Miller, L. L. & Frisbie, C. D. (2003). High electron mobility and ambipolar transport in organic thin-film transistors based on a π-stacking quinoidal terthiophene, *Advanced Materials* **15**(15): 1278–1282.

Cnops, K. (2015). *Phtalocyanine-based Organic Solar Cells and Photodetectors*, PhD thesis, Arenberg Doctoral School.

Colley, N. D. (2016). *COMPUTATIONAL AND EXPERIMENTAL INVESTIGATIONS TOWARDS IMPROVING ORGANIC AND DYE-SENSITIZED SEMICONDUCTOR SOLAR CELLS*, PhD thesis, Southern Illinois University Carbondale.

Cramer, C. J. & Bickelhaupt, F. (2003). Essentials of computational chemistry, *ANGEWANDTE CHEMIE-INTERNATIONAL EDITION IN ENGLISH*- **42**(4): 381–381.

Cravino, A., Leriche, P., Alévêque, O., Roquet, S. & Roncali, J. (2006). Light-emitting organic solar cells based on a 3d conjugated system with internal charge transfer, *Advanced Materials* **18**(22): 3033–3037.

De Leeuw, D., Simenon, M., Brown, A. & Einerhand, R. (1997). Stability of n-type doped conducting polymers and consequences for polymeric microelectronic devices, *Synthetic Metals* **87**(1): 53–59.

Filo, J. & Putala, M. (2010). Semiconducting organic molecular materials, *Journal of Electrical Engineering* **61**(5): 314.

Frisch, M. J., Trucks, G. W., Schlegel, H. B., Scuseria, G. E., Robb, M. A., Cheeseman, J. R.,Scalmani, G., Barone, V., Mennucci, B., Petersson, G. A., Nakatsuji, H., Caricato, M., Li, X.,Hratchian, H. P., Izmaylov, A. F., Bloino, J., Zheng, G., Sonnenberg, J. L., Hada, M., Ehara, M.,Toyota, K., Fukuda, R., Hasegawa, J., Ishida, M., Nakajima, T., Honda, Y., Kitao, O., Nakai, H., Vreven, T., Montgomery, Jr., J. A., Peralta, J. E., Ogliaro, F., Bearpark, M., Heyd, J. J., Brothers,E., Kudin, K. N., Staroverov, V. N., Kobayashi, R., Normand, J., Raghavachari, K., Rendell, A., Burant, J. C., Iyengar, S. S., Tomasi, J., Cossi, M., Rega, N., Millam, J. M., Klene, M., Knox, J. E., Cross, J. B., Bakken, V., Adamo, C., Jaramillo, J., Gomperts, R., Stratmann, R. E., Yazyev, O., Austin, A. J., Cammi, R., Pomelli, C., Ochterski, J. W., Martin, R. L., Morokuma,K., Zakrzewski, V. G., Voth, G. A., Salvador, P., Dannenberg, J. J., Dapprich, S., Daniels, A. D., Farkas, Foresman, J. B., Ortiz, J. V., Cioslowski, J. & Fox, D. J. (n.d.). *Gaussian 09 Revision A.1*. *Gaussian* Inc. Wallingford CT 2009.

Garcia-Belmonte, G., Munar, A., Barea, E. M., Bisquert, J., Ugarte, I. & Pacios, R. (2008). Charge carrier mobility and lifetime of organic bulk heterojunctions analyzed by impedance spectroscopy, *Organic Electronics* **9**(5): 847–851.

Gruhn, N. E., da Silva Filho, D. A., Bill, T. G., Malagoli, M., Coropceanu, V., Kahn, A. & Brédas, J.-L. (2002). The vibrational reorganization energy in pentacene: molecular influences on charge transport, *Journal of the American Chemical Society* **124**(27): 7918–7919.

Gupta, A. (2015). Organic solar cells and its characteristics, *J Material Sci Eng* **4**(203): 2169–0022.

Halsey-Moore, C., Jena, P. & McLeskey Jr, J. T. (2019). Tuning range-separated dft functionals for modeling the peak absorption of meh-ppv polymer in various solvents, *Computational and Theoretical Chemistry* **1162**: 112506.

Hamakawa, Y. (2003). *Thin-film solar cells: next generation photovoltaics and its applications*, Vol. 13, Springer Science & Business Media.

He, Z., Zhong, C., Huang, X., Wong, W.-Y., Wu, H., Chen, L., Su, S. & Cao, Y. (2011). Simultaneous enhancement of open-circuit voltage, short-circuit current density, and fill factor in polymer solar cells, *Advanced Materials* **23**(40): 4636–4643.

Hohenberg, P. & Kohn, W. (1964). Inhomogeneous electron gas, *Physical review* **136**(3B): B864.

Hu, Y., Yin, J., Chaitanya, K. & Ju, X.-H. (2016). Theoretical investigation on charge transfer properties of 1, 3, 5-tripyrrolebenzene (tpb) and its derivatives with electron-withdrawing substituents, *Croatica Chemica Acta* **89**(1): 81–90.

Hutchison, G. R., Ratner, M. A. & Marks, T. J. (2005). Hopping transport in conductive heterocyclic oligomers: reorganization energies and substituent effects, *Journal of the American Chemical Society* **127**(7): 2339–2350.

Jain, A. & Kapoor, A. (2005). A new approach to study organic solar cell using lambert w-function, *Solar energy materials and solar cells* **86**(2): 197–205.

Jayatilaka, D. & Grimwood, D. J. (2003). Tonto: a fortran based object-oriented system for quantum chemistry and crystallography, *International Conference on Computational Science*, Springer, pp. 142–151.

Jenekhe, S. A. & Yi, S. (2000). Efficient photovoltaic cells from semiconducting polymer heterojunctions, *Applied Physics Letters* **77**(17): 2635–2637.

Jin, R. & Wang, K. (2015). Rational design of diketopyrrolopyrrole-based small molecules as donating materials for organic solar cells, *International journal of molecular sciences* **16**(9): 20326–20343.

Jørgensen, M., Norrman, K. & Krebs, F. C. (2008). Stability/degradation of polymer solar cells, *Solar Energy Materials and Solar Cells* **92**: 686–714.

Kietzke, T. (2007). Recent advances in organic solar cells, *Advances in OptoElectronics* **2007**.

Kuo, M.-Y., Chen, H.-Y. & Chao, I. (2007). Cyanation: Providing a three-in-one advantage for the design of n-type organic field-effect transistors, *Chemistry–A European Journal* **13**(17): 4750–4758.

Lee, C., Yang, W. & Parr, R. G. (1988). Development of the colle-salvetti correlation-energy formula into a functional of the electron density, *Physical review B* **37**(2): 785.

Lewars, E. (2003). Computational chemistry, *Introduction to the theory and applications of molecular and quantum mechanics* p. 318.

Li, H., Wang, X. & Li, Z. (2012). Theoretical study of the effects of different substituents of tetrathiafulvalene derivatives on charge transport, *Chinese Science Bulletin* **57**(31): 4049–4056.

Louis, E., San-Fabián, E., Díaz-García, M. A., Chiappe, G. & Vergés, J. A. (2017). Are electron affinity and ionization potential intrinsic parameters to predict the electron or hole acceptor character of amorphous molecular materials?, *The Journal of Physical Chemistry Letters* **8**(11): 2445–2449.

Marcus, R. A. (1964). Chemical and electrochemical electron-transfer theory, *Annual review of physical chemistry* **15**(1): 155–196.

Marcus, R. A. (1993). Electron transfer reactions in chemistry. theory and experiment, *Reviews of Modern Physics* **65**(3): 599.

Markvart, T., McEvoy, A. et al. (2003). *Practical handbook of photovoltaics: fundamentals and applications*, Elsevier.

May, F. (2012). *Charge-transport simulations in organic semiconductors*, PhD thesis, Johannes Gutenberg-University.

McMurry, J. & Simanek, E. (2008). *Fundamentals of organic chemistry*, Beijing: Tsinghua University Press.

Menard, E., Podzorov, V., Hur, S.-H., Gaur, A., Gershenson, M. E. & Rogers, J. A. (2004). Highperformance n-and p-type single-crystal organic transistors with free-space gate dielectrics, *Advanced materials* **16**(23-24): 2097–2101.

Meng, Q. & Hu, W. (2012). Recent progress of n-type organic semiconducting small molecules for organic field-effect transistors, *Physical Chemistry Chemical Physics* **14**(41): 14152–14164.

Nelson, J. (2002). Organic photovoltaic films, *Current Opinion in Solid State and Materials Science* **6**(1): 87–95.

Oshi, R., Abdalla, S. & Springborg, M. (2017). Study of the influence of functionalization on the reorganization energy of naphthalene using dft, *Computational and Theoretical Chemistry* **1099**: 209–215.

Oshi, R., Abdalla, S. & Springborg, M. (2018). Theoretical study on functionalized anthracene and tetraceneas starting species to produce promising semiconductor materials, *Computational and Theoretical Chemistry* **1128**: 60–69.

Oshi, R., Abdalla, S. & Springborg, M. (2019). The impact of functionalization of organic semiconductors by electron donating groups on the reorganization energy, *The European Physical Journal D* **73**(6): 1–8.

Ottonelli, M., Piccardo, M., Duce, D., Thea, S. & Dellepiane, G. (2012). Koopmans' transfer integral calculation: a comparison between the hartree-fock and the density functional results, *Energy Procedia* **31**: 31–37.

Ourahmoun, O. & Belkaïd, M. (2010). Dependence of the characteristics of organic solar cells on cathode polymer interface, *Revue des énergies renouvelables* **13**(4): 583–590.

Peumans, P., Yakimov, A. & Forrest, S. R. (2003). Small molecular weight organic thin-film photodetectors and solar cells, *Journal of Applied Physics* **93**(7): 3693–3723.

Pochettino, A. & Sella, A. (1906). Photoelectric behavior of anthracene, *Acad. Lincei Rend* **15**: 355– 363.

Prabha, A. J., Umadevi, T., Saranyac, P., Maheswari, G. & Meenakshi, R. (2017). A complete theoretical study of indirubin-a blue dye for dye sensitized solar cells (dsscs) applications.

Ramachandran, K., Gopakumar, D. & Namboori, K. (2008). Basis sets, *Computational Chemistry and Molecular Modeling: Principles and Applications* pp. 115–138.

Ray, B., Nair, P. R. & Alam, M. A. (2010). Unraveling the role of morphology on organic solar cell performance, *arXiv preprint arXiv:1011.0956* .

Sahdane, T., Kabouchi, B., Laghrabli, A. & Azize, B. (2017). Photovoltaic energy conversion and optical properties of organic molecules based on aceanthraquinoxaline, *Der Pharma Chemica* **9**(1): 37–42.

Sahoo, S., Parida, S. & Sahu, S. (2016). A theoretical study of charge transport properties of trifluoromethyl (-cf 3) substituted naphthalene (tfmna) molecule, *IOP Conference Series. Materials Science and Engineering (Online)*, Vol. 149.

Sakamoto, Y., Suzuki, T., Kobayashi, M., Gao, Y., Fukai, Y., Inoue, Y., Sato, F. & Tokito, S. (2004). Perfluoropentacene: High-performance p- n junctions and complementary circuits with pentacene, *Journal of the American Chemical Society* **126**(26): 8138–8140.

Sancho-García, J., Pérez-Jiménez, A., Olivier, Y. & Cornil, J. (2010). Molecular packing and charge transport parameters in crystalline organic semiconductors from first-principles calculations, *Physical Chemistry Chemical Physics* **12**(32): 9381–9388.

S. Ashok (n.d.). Solar energy. Encyclopædia Britannica, 2020, accessed October 17, 2020, https://www.britannica.com/science/solar-energy.

Scharber, M. C. & Sariciftci, N. S. (2013). Efficiency of bulk-heterojunction organic solar cells, *Progress in polymer science* **38**(12): 1929–1940.

Selman, N. H. & Mahmood, J. R. (2016). Comparison between perturb & observe, incremental conductance and fuzzy logic mppt techniques at different weather conditions, *International Journal of Innovative Research in Science, Engineering and Technology* **5**(7): 12556–12569.

Simon, P. (2015). Renewable energy medium-term market report 2015. market analysis and forecasts to 2020-executive summary, *International Energy Agency (IEA)* p. 14.

Smith, W. (1873). Effect of light on selenium, *Nature* **7**: 303.

Spackman, P. R., Turner, M. J., McKinnon, J. J., Wolff, S. K., Grimwood, D. J., Jayatilaka, D. & Spackman, M. A. (2021a). Crystalexplorer: A program for hirshfeld surface analysis, visualization and quantitative analysis of molecular crystals, *Journal of Applied Crystallography* **54**(3): 1006– 1011.

Spackman, P. R., Turner, M. J., McKinnon, J. J., Wolff, S. K., Grimwood, D. J., Jayatilaka, D. & Spackman, M. A. (2021b). *CrystalExplorer*: a program for Hirshfeld

surface analysis, visualization and quantitative analysis of molecular crystals, *Journal of Applied Crystallography* **54**(3). **URL:** *https://doi.org/10.1107/S1600576721002910*

Spanggaard, H. & Krebs, F. C. (2004). A brief history of the development of organic and polymeric photovoltaics, *Solar Energy Materials and Solar Cells* **83**(2-3): 125–146.

Stratmann, R. E., Scuseria, G. E. & Frisch, M. J. (1998). An efficient implementation of timedependent density-functional theory for the calculation of excitation energies of large molecules, *The Journal of chemical physics* **109**(19): 8218–8224.

Sukhatme, S. P. & Nayak, J. (2017). *Solar energy*, McGraw-Hill Education.

Sun, C., Li, Y., Song, P. & Ma, F. (2016). An experimental and theoretical investigation of the electronic structures and photoelectrical properties of ethyl red and carminic acid for dssc application, *Materials* **9**(10): 813.

Sun, F. & Jin, R. (2017). DFT and TD-DFT study on the optical and electronic properties of derivatives of 1, 4-bis (2-substituted-1, 3, 4-oxadiazole) benzene, *Arabian Journal of Chemistry* **10**: S2988–S2993.

Tang, C. W. (1986). Two-layer organic photovoltaic cell, *Applied physics letters* **48**(2): 183–185.

Tress, W. (2014). Device physics in a nutshell, *Organic Solar Cells*, Springer, pp. 413–425.

Uchida, S., Xue, J., Rand, B. P. & Forrest, S. R. (2004). Organic small molecule solar cells with a homogeneously mixed copper phthalocyanine: C 60 active layer, *Applied physics letters* **84**(21): 4218– 4220.

Van Thong, P., Chi, N. T. T., Azam, M., Hanh, C. H., Alam, M., Al-Resayes, S. I., Van Hai, N. et al. (2022). Nmr investigations on a series of diplatinum (ii) complexes possessing phenylpropenoids in cdcl3 and cd3cn: Crystal structure of a mononuclear platinum complex, *Polyhedron* **212**: 115612.

Volmer, M. (1913). Die verschiedenen lichtelektrischen erscheinungen am anthracen, ihre beziehungen zueinander, zur fluoreszenz und dianthracenbildung, *Annalen der Physik* **345**(4): 775–796.

Wang, X., Pei, W. & Li, Y. (2020). Enhancing charge transfer and photoelectric characteristics for organic solar cells, *Journal of Nanomaterials* **2020**.

Ward, A. J., Ruseckas, A., Kareem, M. M., Ebenhoch, B., Serrano, L. A., Al-Eid, M., Fitzpatrick, B., Rotello, V. M., Cooke, G. & Samuel, I. D. (2015). The impact of driving force on electron transfer rates in photovoltaic donor–acceptor blends, *Advanced Materials* **27**(15): 2496–2500.

Yanai, T., Tew, D. P. & Handy, N. C. (2004). A new hybrid exchange–correlation functional using the coulomb-attenuating method (cam-b3lyp), *Chemical physics letters* **393**(1-3): 51–57.

Young, D. (2004). *Computational chemistry: a practical guide for applying techniques to real world problems*, John Wiley & Sons.

Yu, G., Gao, J., Hummelen, J. C., Wudl, F. & Heeger, A. J. (1995). Polymer photovoltaic cells: enhanced efficiencies via a network of internal donor-acceptor heterojunctions, *Science* **270**(5243): 1789–1791.

Zaidi, B. (2018). Introductory chapter: Introduction to photovoltaic effect, *Solar Panels and Photovoltaic Materials; InTech Open: London, UK* pp. 1–8.